N-cadherin facilitates trigeminal sensory neuron outgrowth and target tissue innervation

Caroline A. Halmi[1], Carrie E. Leonard[1,3], Alec T. McIntosh[2,3], Lisa A. Taneyhill[1,*]

[1]Department of Animal and Avian Sciences, University of Maryland, College Park, MD 20742 USA

[2]Lombardi Comprehensive Cancer Center, Georgetown University, Washington, DC, 20007 USA

[3]These authors contributed equally to this work.

*Lisa A. Taneyhill
Email: ltaney@umd.edu

Keywords: Trigeminal ganglion, neural crest, placode cells, and N-cadherin.

ABSTRACT

The trigeminal ganglion emerges from the condensation of two distinct precursor cell populations, cranial placodes and neural crest. While its dual cellular origin is well understood, the molecules underlying its formation remain relatively obscure. Trigeminal ganglion assembly is mediated, in part, by neural cadherin (N-cadherin), which is initially expressed by placodal neurons and required for their proper coalescence with neural crest cells. Axon outgrowth first occurs from placodal neurons, but as gangliogenesis proceeds, neural crest cells also differentiate into N-cadherin-expressing neurons, and both extend axons toward targets. However, the role of N-cadherin in axon outgrowth and target innervation has not been explored. Our data show that N-cadherin knockdown in chick trigeminal placode cells decreases trigeminal ganglion size, nerve growth, and target innervation *in vivo*, and reduces neurite complexity of neural crest-derived neurons *in vitro.* Furthermore, blocking N-cadherin-mediated adhesion prevents axon extension in most placodal neurons *in vitro*. Collectively, these findings reveal cell- and non-cell autonomous functions for N-cadherin, highlighting its critical role in mediating reciprocal interactions between neural crest- and placode-derived neurons throughout trigeminal ganglion development.

INTRODUCTION

Sensory ganglia transmit various inputs from the body and environment to the central nervous system (Vermeiren et al., 2020). Within the head, the cranial sensory ganglia perform these functions for their respective cranial nerves. The trigeminal nerve, the largest and most complex of the cranial nerves, relays the majority of somatosensory information within the head (Heimer, 1983) through three major branches - the ophthalmic (OpV), maxillary (MxV), and mandibular (MnV) - that innervate the forehead and eye region, upper jaw, and lower jaw, respectively. The cell bodies for this nerve are positioned within the trigeminal ganglion, which arises from neural crest and placode cells (D'Amico-Martel and Noden, 1980; Hamburger, 1961). While both cell types differentiate into trigeminal sensory neurons (Hamburger, 1961), the neural crest also gives rise to glial cells. Trigeminal neural crest cells originate from the midbrain and anterior hindbrain (Lumsden et al., 1991; Noden, 1973), while the placodal contribution arises from the OpV and maxillomandibular (MmV) placodes. Although these placodes comprise the trigeminal placode to generate one structure, they differ in two important ways. First, they give rise to neurons to distinct lobes of the trigeminal ganglion (OpV versus MxV or MnV, respectively). Second, OpV placode cells begin exiting the cell cycle and differentiating into neurons as early as E1/ Hamburger-Hamilton stage (HH)8 and continue until E3.5/HH21 (McCabe et al., 2009), traveling to the trigeminal ganglion-forming region as a combination of neuroblasts and differentiated neurons. Conversely, the MmV placode generates neuroblasts that do not differentiate or become post-mitotic until they reach the ganglionic anlage (Begbie, 2002; Graham and Shimeld, 2013; McCabe et al., 2009; Shiau et al., 2011). Notably, in the chick, placodal neurons are the first neurons present within the trigeminal ganglion, differentiating and growing towards the periphery to make initial connections with their targets within 2-5 days of development. In contrast, neural crest cells only begin neuronal differentiation at 4 days of development, and continue differentiating up to 7 days (D'Amico-Martel and Noden, 1983, 1980).

Reciprocal interactions between neural crest cells and placodal neurons are required to properly form the trigeminal ganglion (Hamburger, 1961; Moody and Heaton, 1983; Shiau et al., 2008). Much of this research has focused on the influence of neural crest cells on surrounding cell types, but less is known about how placode cells impact the neural crest. Because placodal neurons are present prior to neural crest-derived neurons, they may serve as pioneer neurons, providing a scaffold for later-born neurons to grow along as they innervate their targets (Bate, 1976). Although supported by some studies (Moody et al., 1989; Stainier and Gilbert, 1990), additional evidence for this is needed, and the molecules orchestrating this process remain unknown.

Intercellular adhesion among placode cells and neural crest cells regulates trigeminal gangliogenesis (Steventon et al., 2014) and may also facilitate trigeminal axon outgrowth to targets, with cadherins promoting adhesion between adjacent cells and acting as mediators of gangliogenesis (Halmi et al., 2022; Shiau and Bronner-Fraser, 2009; Theveneau et al., 2013; Wu and Taneyhill, 2019). The cadherin extracellular domain facilitates *cis* and *trans* interactions via homophilic and heterophilic binding (Basu et al., 2017; Halmi et al., 2022; Straub et al., 2011) while the intracellular domain contains two binding sites for catenin proteins (p120-catenin and β-catenin) that regulate cadherin adhesive ability and provide a link to the actin cytoskeleton, respectively (Niessen et al., 2011). Neural cadherin (N-cadherin) is expressed in neural tissue at various stages of development (Hatta and Takeichi, 1986). It is also found in mesodermal (Dady et al., 2012; Nakagawa and Takeichi, 1997) and ectodermal derivatives, including trigeminal and epibranchial placode cells prior to their delamination (Shiau and Bronner-Fraser, 2009), and later in all trigeminal sensory neurons (Inuzuka et al., 1991; Itoh et al., 1997; Redies et al., 1992; Tan et al., 2010). While multiple studies, largely in the central nervous system, describe roles for N-cadherin in regulating neurite formation (Bixby and Zhang, 1990; Gärtner et al., 2012; Hansen et al., 2008), axon fasciculation (Masai et al., 2003), and synapse formation (Benson and Tanaka, 1998; Jontes, 2018; Riehl et al., 1996), the function of N-cadherin in sensory neurons has not been thoroughly characterized. Although N-cadherin function in

125 placode cells is critical for the early condensation of the chick trigeminal ganglion
126 from undifferentiated neural crest cells and placodal neurons (Shiau and Bronner-
127 Fraser, 2009), whether N-cadherin mediates the later growth and maturation of all
128 trigeminal ganglion sensory neurons, and specifically neurite production and axon
129 extension, is unknown. Furthermore, how N-cadherin-expressing placodal
130 neurons impact the development of later-born neural crest-derived neurons is
131 poorly understood.

132 Building upon these prior studies, we demonstrate that placodal expression
133 of N-cadherin is vital for later chick trigeminal neurodevelopment. We observed
134 substantial deficits in trigeminal ganglion morphology and axonal projections to
135 target tissues that arise from effects on both placode- and neural crest-derived
136 neurons in response to N-cadherin depletion from placodal neurons. These latter
137 defects are noted both *in vivo* and *in vitro,* providing evidence to support the
138 hypothesis that N-cadherin-mediated adhesion is important for trigeminal
139 neurodevelopment. Strikingly, we note decreased neurite production in neural
140 crest-derived neurons that correlates with altered β-catenin levels, pointing to non-
141 cell autonomous effects on the neural crest after N-cadherin knockdown in
142 placodal neurons. These results indicate that trigeminal neurons depend on the
143 adhesive function of N-cadherin to facilitate the outgrowth of axons. Altogether,
144 our findings reveal a new long-term role for N-cadherin in driving the proper
145 outgrowth of both placode- and neural crest-derived neurons throughout trigeminal
146 gangliogenesis.
147

148 **RESULTS**

149 **N-cadherin knockdown in placode cells disrupts trigeminal ganglion**
150 **development**

151 To elucidate the function of N-cadherin in placodal neurons during the
152 formation and maturation of the trigeminal ganglion, a validated N-cadherin
153 morpholino (Shiau and Bronner-Fraser, 2009) (MO) was unilaterally
154 electroporated into chick trigeminal placode cells at a single timepoint prior to their
155 delamination. Embryos were grown to various endpoints (2.5-6.5 days post-
156 incubation) to assess trigeminal ganglion morphology. Initial experiments with a 5

157 base pair mismatch N-cadherin control MO (N-cadherin MM) (Shiau and Bronner-
158 Fraser, 2009) confirmed that the electroporation technique did not cause any
159 morphological changes (Fig. S1). Once validated, the unelectroporated
160 (contralateral) sides of N-cadherin MO-electroporated embryos were used as
161 controls for all *in vivo* experiments to account for any developmental variation.
162 Trigeminal ganglion size and nerve morphology were analyzed by whole-mount
163 immunohistochemistry using an antibody against tubulin beta 3, class III (Tubb3)
164 to label neurons, followed by tissue clearing for imaging. Given the time difference
165 in neuronal differentiation in the trigeminal ganglion (D'Amico-Martel and Noden,
166 1983; Moody et al., 1989), the Tubb3 antibody was presumed to identify placode-
167 derived neurons up to E4/HH23, after which both placode- and neural crest-
168 derived neurons were labeled indistinguishably.

169 During initial gangliogenesis (E2.5/HH16-18), N-cadherin depletion from
170 trigeminal placode cells caused neuron dispersal, increasing the forming trigeminal
171 ganglion area compared to the contralateral control (Fig. 1A-A', 1F), consistent
172 with previous work (Shiau and Bronner-Fraser, 2009). However, by E3.5/HH19-
173 22, the size of the trigeminal ganglion on the electroporated side was significantly
174 reduced compared to the contralateral control (Fig. 1B-B', 1F). This reduction
175 persisted even as neural crest cells began differentiating into neurons at
176 E4.5/HH23-25 (Fig. 1C-C', 1F), pointing to potential effects on both placode- and
177 neural crest-derived neurons during trigeminal neurodevelopment. At both
178 E5.5/HH26-27 and E6.5/HH28-30, N-cadherin MO-electroporated trigeminal
179 ganglia were no longer statistically different from controls (Fig. 1D-E', 1F).

180 Next, we measured the area of OpV and MmV individually. Interestingly, N-
181 cadherin knockdown led to a significant increase in MmV, but not OpV, at
182 E2.5/HH16-18 (Fig. 1G-H). However, from E3.5-E6.5/HH19-30, N-cadherin
183 depletion did not affect MmV lobe development (Fig. 1H) but led to a significant
184 reduction in OpV lobe size (Fig. 1D-D', 1G). By E6.5/HH28-30, the size of both
185 lobes was similar to controls (Fig. 1G-H). We did not observe any increased cell
186 proliferation in N-cadherin MO OpV lobes at E6.5/HH28-30, as indicated by

187 phospho-histone H3 expression (Fig. S2), that would explain the absence of
188 phenotype observed at this stage.

189 To investigate whether specific subpopulations of trigeminal sensory
190 neurons were being impacted after N-cadherin knockdown, we analyzed TrkA and
191 TrkB receptor expression in OpV sections at E5.5/HH26-27 when both placode-
192 and neural crest-derived neurons are present in the trigeminal ganglion, as this
193 stage grouping include neural crest cell differentiation into neurons (D'Amico-
194 Martel and Noden, 1983; Williams et al., 1995). TrkA and TrkB neurons were
195 counted on immunolabeled sections from contralateral (Fig. S3A-B') and N-
196 cadherin MO (Fig. S3C-D') trigeminal ganglia. N-cadherin MO treatment caused a
197 significant decrease in TrkB-positive neurons (Fig. S3E); however, after
198 normalization against the smaller area of the OpV lobe, the TrkB neuron count was
199 no longer statistically different from controls (Fig. S3F). No changes were observed
200 in TrkA-positive neurons (Fig. S3E-F). These results suggest that the
201 morphological deficits observed in the trigeminal ganglion over time cannot be
202 attributed to alterations in specific neuronal subpopulations.
203

204 **Depletion of N-cadherin from trigeminal placode cells disrupts target**
205 **innervation by OpV nerves**

206 Since extensive morphology changes were observed within OpV (Fig. 1G-
207 H), we focused subsequent *in vivo* analyses on its development and next
208 evaluated whether OpV axons and nerve projections into cranial target tissues
209 were also affected. We first examined the lateral nasal branch at E4.5/HH23-25,
210 as it becomes a prominent structure within the embryonic head by this stage
211 (Higashiyama and Kuratani, 2014). We performed whole-mount Tubb3
212 immunohistochemistry, which labels both placode- and neural crest-derived
213 neurons at this stage, and compared the N-cadherin MO-electroporated side of the
214 embryo to the contralateral control side. These experiments revealed fewer lateral
215 nasal nerve branches on the N-cadherin MO side of the embryo (Fig. 2A-B). To
216 quantify these findings, we assessed the distribution of terminal nerve endings at
217 30 μm intervals, starting at the first axon branching point from the OpV lobe. No

218 difference in the number of terminal nerve endings was observed closer to the
219 trigeminal ganglion, but fewer were present in distal regions after N-cadherin MO
220 treatment (Fig. 2C). Moreover, nerve width and innervation area were significantly
221 reduced after N-cadherin knockdown compared to contralateral control trigeminal
222 ganglia (Fig. 2D-E).

223 Using the same method, we evaluated the medial nasal nerve at
224 E5.5/HH26-27, as this stage provided more consistent morphological development
225 compared to E4.5/HH23-25 embryos (Higashiyama and Kuratani, 2014), where
226 increased variability was observed. While the number of medial nasal terminal
227 nerve endings was similar between conditions (Fig. 2F-H), the nerve width and
228 target innervation area were significantly smaller after N-cadherin knockdown
229 compared to contralateral control trigeminal ganglia (Fig. 2I-J). Together, these
230 findings reveal that N-cadherin is required by OpV trigeminal neurons to send
231 axons to targets, thus leading to proper nerve outgrowth, fasciculation, and target
232 innervation.

233

234 **N-cadherin knockdown in placode cells leads to increased cell death within**
235 **the OpV lobe**

236 To assess whether cell death altered OpV lobe size, axon outgrowth, and
237 target innervation after N-cadherin knockdown in placode cells, we performed
238 staining for apoptotic cells using cleaved caspase-3 and TUNEL (Fig. 3). We
239 examined timepoints encompassing when placode cells are first delaminating
240 (E1.5/HH13-15) and when morphological changes were observed (Fig. 1:
241 E2.5/HH16-18, E3.5/HH19-22, E4.5/HH23-25). Apoptosis was evident in tissue
242 sections from unelectroporated, contralateral control (Fig. 3A-A') and N-cadherin
243 MO-electroporated (Fig. 3B-B') trigeminal ganglia. When correcting for size
244 differences in the ganglion after N-cadherin knockdown, cell death was
245 significantly increased on the N-cadherin MO-treated side only during initial
246 coalescence of placodal neurons with undifferentiated neural crest cells
247 (E2.5/HH16-18), when OpV size remained unchanged (Fig. 1A-A', 1G). Once
248 placodal neurons and neural crest cells have formed the trigeminal ganglion, and

249 neural crest cells have begun differentiating into neurons beyond E4, there was no
250 significant difference in cell death between the N-cadherin MO-treated and
251 contralateral control sides (Fig. 3C), despite reduced OpV size at these stages
252 after N-cadherin knockdown (Fig. 1B-D', 1G). These data suggest that apoptosis
253 could partially account for some of the morphological phenotypes observed during
254 early gangliogenesis prior to neural crest cell differentiation into trigeminal sensory
255 neurons.
256

257 **Neurite complexity in neural crest-derived neurons is reduced after N-**
258 **cadherin knockdown in placode cells**

259 The absence of persistent apoptosis and presence of continued axon
260 outgrowth deficits, particularly at stages when neural crest cells differentiate into
261 neurons, led us to hypothesize that depletion of N-cadherin from placode cells may
262 be impacting later-born neural crest-derived neurons. To test this, we performed a
263 sequential electroporation (Halmi et al., 2022) using a genome-incorporating
264 vector (PiggyBacGFP) and its accompanying transposase (PBase) (Lu et al.,
265 2009; Macdonald et al., 2012) to first label neural crest cells with a stably
266 expressed green fluorescent protein (GFP), followed by electroporation of placode
267 cells with N-cadherin MO or the validated N-cadherin mismatch (MM) control
268 morpholino (Fig. S1), which was used as the control for this experiment (Shiau
269 and Bronner-Fraser, 2009). Sequential electroporations of neural crest cells and
270 placode cells leads to mutually exclusive expression of the introduced
271 plasmid/morpholino (Fig. S4), as shown previously (Halmi et al., 2022).
272 Sequentially-labeled trigeminal ganglia were dissected, cultured as explants,
273 grown *in vitro* for 3 days, and subsequently processed for immunostaining with
274 GFP and Tubb3 antibodies (Fig. 4A). Although N-cadherin MM-treated explant
275 cultures exhibited numerous axons extending from neural crest-derived neurons
276 (Fig. S5A-A'), qualitatively we observed relatively few GFP-positive neural crest-
277 derived axons in N-cadherin MO-treated samples (Fig. S5B-B'). Interestingly,
278 neurites, which precede axon specification and extension (Sainath and Gallo,
279 2015), were noted from GFP-positive neural crest-derived somata in both N-

280 cadherin MO- and N-cadherin MM-treated explant cultures. These were numerous
281 in N-cadherin MM-treated explant cultures (Fig. 4B-C), but noticeably fewer in N-
282 cadherin MO-treated explants (Fig. 4D-E). In addition to a significant decrease in
283 the number of primary and secondary neurites in neural crest-derived neurons,
284 tertiary neurites were absent in N-cadherin MO-treated samples but present in N-
285 cadherin MM-treated explants (Fig. 4F). Although neurite branching was deficient
286 in N-cadherin MO-treated explants cultures, there was no difference in the length
287 of primary and secondary neurites compared to N-cadherin MM-treated explant
288 cultures (Fig. 4G). These results indicate that N-cadherin in placodal neurons non-
289 cell autonomously facilitate axon extension and branching in neural crest-derived
290 neurons *in vitro*, providing an additional explanation for the sustained
291 morphological deficits noted in the trigeminal ganglion *in vivo*.
292 To explore a potential mechanism behind this observation, we examined β-
293 catenin within neural crest-derived neurons in this same assay, given its known
294 interactions with N-cadherin and role in neurite outgrowth (Benson and Tanaka,
295 1998; Halbleib and Nelson, 2006; Miyamoto et al., 2015). While membranous β-
296 catenin was evident in neural crest-derived neurons of N-cadherin MM-treated
297 samples (Fig. 4H, arrowheads), β-catenin levels were significantly reduced in
298 neural crest-derived neurons of N-cadherin MO-treated samples, with less β-
299 catenin evident along cell membranes (Fig. 4I, 4J). These findings support a
300 mechanism whereby changes to β-catenin levels could contribute to the defects
301 observed in neural crest-derived neurite production after N-cadherin knockdown in
302 placode cells.

303 **N-cadherin controls proper axon outgrowth of trigeminal neurons *in vitro***

304 The morphological defects observed after N-cadherin knockdown in
305 placode cells *in vivo* and *in vitro* suggest a role for N-cadherin-mediated adhesion
306 in facilitating axon outgrowth of both placode- and neural crest-derived trigeminal
307 sensory neurons. To test this, we utilized a validated function-blocking antibody
308 against the extracellular domain of N-cadherin, known as MNCD2 (Bronner-Fraser
309 et al., 1992; Redies et al., 1992) (anti-N-cadherin), to block N-cadherin-mediated
310 adhesion in explanted trigeminal ganglion tissue.

311 Trigeminal ganglion explant cultures were grown *in vitro* for 24 hours,
312 followed by treatment with anti-N-cadherin or a control rat IgG antibody for an
313 additional 24 hours (Fig. 5A), and then processed for Tubb3 immunostaining (Fig.
314 5B, C, D). Wildtype explants incubated *in vitro* for 24 hours without treatment
315 served as controls ("pre-treatment") to evaluate baseline axon outgrowth and the
316 possibility of axon pruning prior to antibody treatment. Ridge detection was used
317 to detect segments, which were used as a proxy for individual axons (Fig. 5B', C',
318 D'), and an intersection analysis was run to measure changes to axon outgrowth
319 and branching (Fig. 5B", 5C", D"). While the Tubb3 fluorescence intensity between
320 pre-treatment explants and anti-N-cadherin-treated samples was similar, a 60%
321 reduction in Tubb3 fluorescence was observed in anti-N-cadherin-treated samples
322 compared to rat IgG-treated samples (Fig. 5E). These results point to decreased
323 axon density in trigeminal ganglion explant cultures after blocking N-cadherin-
324 based adhesion. Furthermore, intersection analyses revealed that explants treated
325 with anti-N-cadherin exhibited a significant increase in axonal branching compared
326 to pre-treatment samples up to 1400 μm, while rat IgG-treated explants exhibited
327 a significant increase in branching up to 1750 μm compared to the pre-treatment
328 group (Fig. 5F). However, when comparing the anti-N-cadherin- and rat IgG-
329 treated explants, significant differences were only observed up to 700 μm (Fig. 5F).
330 Interestingly, of the neurons that did extend axons, the mean segment
331 length of detected axons was similar between pre-treatment and anti-N-cadherin-
332 treated explants (Fig. 5G), suggesting that some axons can extend in the absence
333 of N-cadherin-mediated adhesion. However, the rat IgG-treated group had a
334 significantly decreased average segment length compared to both, providing
335 further support for increased axon branching over time. To verify this and confirm
336 that the decreased segment length was not due to axon pruning, we visualized all
337 detected segments using a violin plot to assess the distribution of the data (Fig.
338 5H). This analysis confirmed an increase in smaller segments in the rat IgG-treated
339 group, validating that the observed decrease in mean segment length (Fig. 5G)
340 resulted from averaging long and short segments, rather than axons retracting over
341 time. Collectively, these data suggest N-cadherin-mediated adhesion promotes

342 axonal outgrowth and complexity in trigeminal neurons *in vitro* but does not likely
343 function in axon trimming.
344
345 **N-cadherin is required cell autonomously for the axon outgrowth of the**
346 **majority of placodal neurons**
347 Our preceding findings indicate that most trigeminal sensory neurons rely
348 on N-cadherin for axon outgrowth. To investigate their cellular origin, an
349 ectodermal co-electroporation with a stably expressed red fluorescent protein
350 (PiggyBacRFP plus PBase) (Lu et al., 2009; Macdonald et al., 2012) was
351 performed to label placode-derived neurons. Next, RFP-positive explant cultures
352 were treated with either rat IgG or anti-N-cadherin as previously described.
353 Following immunostaining with Tubb3 and RFP antibodies, robust axon outgrowth
354 was observed, the majority of which overlapped with RFP-positive placode-derived
355 neurons after rat IgG treatment (Fig. 6A). Many Tubb3-positive projections were
356 also RFP-positive in these control explant cultures (Fig. 6B-B"). Explant cultures
357 treated with anti-N-cadherin, however, exhibited reduced overall axon outgrowth
358 and fewer RFP-positive projections (Fig. 6C), as noted previously (Fig. 5C). While
359 colocalization of Tubb3 and RFP was maintained in the anti-N-cadherin-treated
360 axonal projections, the total amount of outgrowth was less (Fig. 6D-D").
361 Importantly, although overall Tubb3 fluorescence was significantly reduced in the
362 anti-N-cadherin-treated explant cultures, reflecting fewer axons observed after
363 blocking N-cadherin-mediated adhesion, there was no change in RFP protein
364 (fluorescence, Fig. 6E) or *RFP* transcript (Fig. 6F) levels between the treatments.
365 These findings reveal that blocking N-cadherin-mediated adhesion did not affect
366 the presence of placodal neurons, but rather impacted axon outgrowth.
367 Given these data and our prior results pointing to a role for N-cadherin in
368 axon outgrowth, we hypothesized that anti-N-cadherin-treated explant cultures
369 would show a greater amount of RFP signal within the core of the explanted tissue,
370 which contains the majority of the neuronal cell bodies, due to the increased
371 presence of placodal neurons unable to extend axons in the absence of N-
372 cadherin-mediated adhesion. To address this, we evaluated the RFP signal found

373 in axonal projections versus RFP signal remaining within the core of the explanted
374 tissue (Fig. 6G). While 33% of the total RFP signal came from axonal projections
375 in rat IgG-treated explants, this dropped to 15% in anti-N-cadherin-treated
376 explants. In contrast, 67% of the total RFP signal was found in the core of the rat
377 IgG-treated explants versus 85% in anti-N-cadherin-treated explants (Fig. 6H).
378 Taken together, these data highlight a cell-autonomous requirement for N-
379 cadherin-mediated adhesion in the proper axon outgrowth of placode-derived
380 neurons.
381

382 **Inhibiting N-cadherin-mediated adhesion diminishes neurite complexity in**
383 **neural crest-derived neurons**

384 Due to the changes we observed in RFP-labeled placodal neurons after
385 blocking N-cadherin-mediated adhesion, we next chose to assess whether neural
386 crest-derived neurons were also impacted. To test this, a neural tube
387 electroporation was performed with PiggyBacGFP with PBase to label the neural
388 crest cells. Next, GFP-positive explant cultures were treated with either rat IgG or
389 anti-N-cadherin as previously described (Fig. 7A), immunostained with a GFP
390 antibody, and neurites were traced (Fig. 7B-C'). Similar to our previous results after
391 N-cadherin MO treatment (Fig. 4), we observed a decrease in neurite complexity
392 after anti-N-cadherin treatment. Neural crest-derived neurons showed a significant
393 reduction in both primary and secondary neurites compared to rat IgG-treated
394 explants (Fig. 7D). In line with our results from Figure 4, we did not observe a
395 change in the average neurite length of primary neurites between treatment groups
396 (Fig. 7E). Very few anti-N-cadherin-treated neural crest-derived neurons had
397 secondary or tertiary neurites, preventing analyses of neurite length. These
398 findings reveal that the adhesive role of N-cadherin impacts the ability of neural
399 crest-derived neurons to generate complex neurites.
400

401 **DISCUSSION**

402 Here we demonstrate a sustained role for N-cadherin during trigeminal
403 gangliogenesis, emphasizing the need for cell-cell adhesion in the formation and

404 maturation of the OpV lobe of the trigeminal nerve. Our findings show that reducing
405 N-cadherin from trigeminal placode cells and their neuronal derivatives disrupts
406 trigeminal ganglion morphology and target innervation by specific OpV nerve
407 branches. We found that neural crest-derived neurons rely on N-cadherin in
408 placodal neurons for proper neurite outgrowth and that β-catenin levels are
409 reduced in them after N-cadherin knockdown in placode cells. Moreover, blocking
410 N-cadherin-mediated adhesion led to similar effects, suggesting this underpins the
411 *in vivo* phenotypes observed. These results highlight the continued role of N-
412 cadherin for sensory neurodevelopment and reinforce the importance of reciprocal
413 interactions between placode cells and neural crest cells during cranial ganglia
414 formation.
415
416 **Depletion of N-cadherin from placodal neurons leads to persistent**
417 **morphological defects in the developing trigeminal ganglion**
418 N-cadherin in placode cells plays important roles during early cranial
419 ganglia formation, including facilitating collective cell migration through a repulsive
420 "chase and run" mechanism (Theveneau et al., 2013) and the coalescence of
421 undifferentiated neural crest cells and placodal neurons to generate the trigeminal
422 ganglion (Shiau and Bronner-Fraser, 2009). However, its role in regulating axon
423 extension for proper target innervation has not been explored. Our experiments
424 showed that N-cadherin knockdown initially increased ganglion area, replicating
425 previous results (Shiau and Bronner-Fraser, 2009), but then led to a reduction in
426 trigeminal ganglion size up to E4.5, which eventually recovered. We believe there
427 are two potential reasons for this recovery. First, MOs are typically only stable for
428 up to 4-5 days *in vivo*, reflecting a limitation of our technique (Bill et al., 2009).
429 Therefore, it is possible that at the later timepoints, the MO was targeted for
430 degradation, minimizing phenotypic effects. However, we think this is unlikely, or
431 plays a minimal role, as reduced N-cadherin protein levels were still observed at
432 E6.5/HH28-30. Second, the continued differentiation of neural crest cells into
433 neurons and glia beyond E4-5/HH24-27 (D'Amico-Martel and Noden, 1980) may

434 compensate for this decrease in trigeminal ganglion size, which would not be
435 discernable by Tubb3 immunostaining alone.
436 In keeping with previous studies, we observed more pronounced
437 phenotypes in OpV compared to MmV, possibly due to the earlier differentiation of
438 OpV neurons compared to MmV cells, which remain proliferative until later stages
439 (Begbie, 2002; Graham and Shimeld, 2013; Lassiter et al., 2014; McCabe et al.,
440 2009; Stark et al., 1997). Although this could be caused by the mosaic nature of
441 the electroporation, we suspect this difference is most likely attributed to MO
442 dilution over time in MmV. OpV placode cells are the first to express neuron-
443 specific markers and become post-mitotic, some even before leaving the ectoderm
444 (McCabe et al., 2009), resulting in more prominent phenotypes. Conversely, MmV
445 placode cells remain as proliferative neuroblasts until after delamination (Begbie,
446 2002; Graham and Shimeld, 2013; McCabe et al., 2009). N-cadherin depletion
447 from placode cells showed the greatest size difference in OpV at E3.5/HH19-22,
448 coinciding with when the majority of placodal neurons have initiated axon
449 outgrowth (Moody et al., 1989), while no change was observed by E6.5/HH28-30.
450 This suggests that N-cadherin plays a role in promoting axon outgrowth during
451 early stages of neurodevelopment. Notably, we did not observe changes to TrkA-
452 and TrkB-expressing cells when these neurons are prominent (E5.5/HH26-27),
453 indicating altered neuronal differentiation was not a factor in the morphological
454 effects observed. Interestingly, N-cadherin protein levels were still reduced in OpV
455 at E6.5/HH28-30, suggesting continuing effects on N-cadherin even if the MO was
456 targeted for degradation. Additionally, we observed a decrease in cell division in
457 OpV in this stage grouping after N-cadherin knockdown, pointing to other
458 mechanisms that compensate for the absence of phenotype. As only a neuronal
459 marker (Tubb3) was used in these experiments, it is possible that the balance of
460 neural crest cell differentiation into neurons vs. glia was affected, leading to more
461 of the former over the latter.
462
463

464 **Reducing N-cadherin in placodal neurons impacts OpV nerve innervation**
465 **patterns**

466 Further studies revealed a requirement for N-cadherin in the lateral and
467 medial nasal branches of OpV, with the former exhibiting more drastic changes
468 upon N-cadherin MO treatment. The lateral nasal branch exhibited decreased
469 terminal nerve branches, reduced nerve width, and a smaller innervation area,
470 while the medial nasal nerve showed similar trends for nerve width and innervation
471 area, albeit to a lesser extent. Interestingly, there was no change in the number of
472 terminal nerve branches in the medial nasal branch. This contrasting result - a
473 smaller nerve bundle having similar axonal branching - suggests that N-cadherin
474 functions to adhere individual axons with each other at medial nasal branch
475 targets. Similar phenotypes after N-cadherin perturbations have been observed in
476 other systems as well (Reis et al., 2011; Shikanai et al., 2018; Tan et al., 2010).

477 Although both OpV branches begin developing at similar stages
478 (Higashiyama and Kuratani, 2014), we chose to examine the E5.5/HH26-27
479 timepoint for the medial nasal nerve studies due to more consistency among
480 embryos. While differences in embryo age could explain the varying results
481 between the nerve branches, it is equally plausible that the proportion of N-
482 cadherin-expressing placodal neurons differs between them, as the contribution of
483 neural crest- and placode-derived neurons to these nerve branches is unknown.
484 Further, the differences observed could be due to when the respective branches
485 form, as our results suggest that medial nasal branch development occurs after
486 the lateral nasal branch. If true, knockdown of N-cadherin would preferentially
487 impact the lateral nasal nerve since it develops first. Alternatively, the mosaic
488 nature of the electroporation technique may also explain these phenotypes.
489

490 **N-cadherin in placodal neurons functions non-cell autonomously to control**
491 **neurite production in neural crest-derived neurons**

492 Given the observed alterations to trigeminal ganglion morphology, we
493 investigated whether increased apoptosis contributed to these phenotypes.
494 Although our Tubb3 immunohistochemistry results showed no size difference in

495 OpV at the first timepoint examined (E2.5/HH16-18), a significant increase in
496 apoptosis was detected at this timepoint. This suggests that, while the same
497 number of cells may initially contribute to the forming ganglion, some undergo
498 apoptosis, potentially impacting OpV size at later stages and contributing to the
499 long-term phenotypes seen in our studies. However, the absence of any increased
500 apoptosis at later stages, particularly when neural crest cells are differentiating into
501 neurons, implies other mechanisms are also involved.

502 To address this, we evaluated axon outgrowth of neural crest-derived
503 neurons. Fluorescent labeling of neural crest cells followed by N-cadherin MO
504 treatment in placode cells revealed very few neural crest-derived axons. The
505 complexity of neurites in these neurons was significantly reduced, indicating non-
506 cell autonomous effects. This highlights the continued importance of N-cadherin-
507 mediated interactions throughout trigeminal gangliogenesis, particularly between
508 placode- and neural crest-derived neurons. N-cadherin functions in neurite
509 production for other peripheral neurons (Bixby and Zhang, 1990), and its
510 localization at specific sites along the cell membrane precedes neurite formation
511 (Gärtner et al., 2012). Depletion of N-cadherin from placodal neurons could
512 prevent *trans* N-cadherin interactions between neural crest cells/neural crest-
513 derived neurons and placodal neurons, disrupting neurite production. Additionally,
514 since N-cadherin is also involved in dendrite maintenance (Tan et al., 2010), the
515 stability of neural crest-derived neurites may be compromised when N-cadherin is
516 knocked down in placodal neurons. Interestingly, despite fewer neurites observed
517 in N-cadherin MO-treated explants, neurite length remained the same between
518 treatments, suggesting that processes controlling neurite length are unaffected by
519 knockdown of N-cadherin in placode cells.

520 Irrespective of the mechanism behind reduced neurite formation,
521 disruptions to the cytoskeleton are likely involved. Our studies revealed a decrease
522 in β-catenin in neural crest-derived neurons upon knockdown of N-cadherin in
523 placode cells. Membrane-bound N-cadherin regulates the availability of both β-
524 catenin and p120-catenin for binding and activating various signaling pathways
525 (Radice, 2013). If *trans* N-cadherin interactions among neural crest- and placode-

526 derived neurons are disrupted, β-catenin could be impacted, leading to the loss of
527 intracellular signaling required to activate GTPases and other cytoskeletal
528 proteins, thus impacting neurite production. Finally, cadherin-receptor tyrosine
529 kinases interactions at cellular membranes reportedly regulate each other
530 (Chiasson-MacKenzie and McClatchey, 2018), including those between N-
531 cadherin and Fibroblast Growth Factor receptors (Hansen et al., 2008; Nguyen
532 and Mège, 2016), which may be critical for the proper growth, maturation, and
533 survival of neural crest-derived neurons. Disrupting N-cadherin levels could
534 interfere with these interactions, affecting the proper development of these
535 neurons.
536
537 **N-cadherin-mediated adhesion facilitates axon outgrowth of placode- and**
538 **neural crest-derived trigeminal neurons**
539 To elucidate whether the *in vivo* phenotypes were due to loss of N-cadherin-
540 dependent adhesion, we used a function-blocking antibody to broadly inhibit N-
541 cadherin in trigeminal ganglion explant cultures. Three main conclusions emerged
542 from the analysis. First, blocking N-cadherin-mediated adhesion did not preclude
543 axon outgrowth. Second, intersection analyses revealed reduced axon outgrowth
544 and branching in anti-N-cadherin-treated explants compared to rat IgG-treated
545 controls. However, anti-N-cadherin-treated explants still extended axons to the
546 periphery, though not significantly more than pre-treatment explants, suggesting
547 some axons may be retracting, due to either pruning or lack of necessary factors
548 in the media to support axon maintenance. Lastly, segment lengths (used as a
549 proxy for axons) were significantly reduced in our rat IgG-treated explants
550 compared to both pre-treatment and anti-N-cadherin-treated explants. This
551 reduction was due to a higher number of very short segments in the rat IgG group,
552 as longer axon lengths were observed in all groups and argues against a
553 substantial role for axon pruning. Since some trigeminal neurons could extend
554 axons similarly to controls despite N-cadherin inhibition, we conclude that N-
555 cadherin is not essential for axon outgrowth in all trigeminal neurons. These data
556 align with the *in vivo* observation for OpV branches in that N-cadherin knockdown

557 does not completely block target innervation but reduces the number of axons
558 reaching their targets. While this phenotype could be attributed to the mosaic
559 nature of the MO electroporation, our *in vitro* results now offer another potential
560 explanation, in that some neurons are not reliant on N-cadherin for the outgrowth
561 of their axons.

562 We next identified the cellular origin of the neurons requiring N-cadherin-
563 mediated adhesion for their outgrowth, hypothesizing that they would be placode-
564 derived since placode cell neuronal differentiation precedes neural crest cell
565 differentiation *in vivo* (D'Amico-Martel and Noden, 1983). Our experiments showed
566 reduced axon outgrowth in RFP-labeled placodal neurons after anti-N-cadherin-
567 treatment. Although some neurons might have initially extended axons and then
568 died, we believe this is unlikely because a subset of neurons was always capable
569 of growing axons irrespective of when the anti-N-cadherin antibody was added to
570 the explants. Although RFP transcript and protein levels were similar between
571 treatments, very interestingly, RFP signal in axonal projections was reduced after
572 anti-N-cadherin treatment, with most RFP signal originating from inside the cores.
573 This indicates that N-cadherin promotes axon outgrowth, with its absence limiting
574 the number of RFP-positive placodal neurons capable of extending axons.

575 Although we did not observe interactions between fluorescently labeled
576 placodal neurons and neural crest-derived neurons *in vitro* upon blocking N-
577 cadherin-mediated adhesion, we did see changes in neurite production of neural
578 crest-derived neurons. While both primary and secondary neurite number was
579 significantly reduced, neurite length remained unchanged across treatments.
580 These results mirrored phenotypes in neural crest-derived neurons when N-
581 cadherin was knocked down from placode cells, indicating that the loss of N-
582 cadherin from placodal neurons impacts the ability of neural crest-derived neurons
583 to produce neurites. This likely contributes to the reduced size of the trigeminal
584 ganglion observed in N-cadherin knockdown embryos, as these neurons may be
585 unable to extend axons to their targets properly.

586 Surprisingly, a small subset of RFP-positive placodal neurons exhibited
587 axon outgrowth after anti-N-cadherin treatment, potentially representing pioneer

588 neurons of the trigeminal ganglion. Though pioneer neurons are well-documented
589 in invertebrate models (Clarke et al., 2020; Hidalgo and Brand, 1997; Klose and
590 Bentley, 1989; Lin et al., 1995), evidence in vertebrates (Eisen et al., 1986; Ghosh
591 et al., 1990; Gong and Shipley, 1995), including in mouse trigeminal
592 neurodevelopment, suggests that the first axons to extend from OpV provide a
593 path for secondary axons to reach their targets (Stainier and Gilbert, 1990). A
594 similar phenomenon has been observed in the chick trigeminal ganglion, where a
595 few placode-derived neurons were observed to extend axons to the periphery,
596 providing a path for later-born neurons to follow (Moody et al., 1989). Collectively,
597 these studies and our new data suggest that a subset of placodal neurons may
598 serve as pioneers upon which other placode-derived neurons and later neural
599 crest-derived neurons ("followers") extend axons (Moody et al., 1989). This N-
600 cadherin-independent (pioneer) and -dependent (follower) outgrowth is
601 reminiscent of mechanisms regulating migration in the facial branchiomotor neuron
602 system (Wanner and Prince, 2013).
603

604 **CONCLUSION**

605 In this study, we have shown a sustained negative impact on the trigeminal
606 ganglion following N-cadherin depletion from placodal neurons. Throughout
607 development, including after neural crest cells differentiate into neurons, we
608 observed changes in trigeminal ganglion size and reduced axon outgrowth to
609 target tissues. These morphological differences could not be fully explained by
610 increased apoptosis. In support of this, neurite production and β-catenin levels in
611 neural crest-derived neurons were altered after depleting N-cadherin from placode
612 cells. Treatment of explants with an N-cadherin adhesion-blocking antibody
613 caused similar effects on neurites, pointing to a non-cell autonomous requirement
614 for N-cadherin in placodal neurons to facilitate axon outgrowth from placode- and
615 neural crest-derived trigeminal neurons. Inhibiting N-cadherin-mediated adhesion
616 *in vitro* also reduced axon outgrowth from most placodal neurons, demonstrating
617 a cell autonomous function for N-cadherin in this process. Altogether, our results
618 add to the growing amount of evidence supporting the importance of reciprocal
619 interactions between neural crest cells and placode cells during the formation of
620 the cranial ganglia, and highlight a long-term, critical role for N-cadherin during
621 trigeminal gangliogenesis that will likely be translatable to other cranial ganglia and
622 vertebrate species.

623

624

625

626 **MATERIALS AND METHODS**
627
628 **Chick embryos**
629 Fertilized chicken eggs (*Gallus gallus*) were obtained from the Department
630 of Animal and Avian Sciences at the University of Maryland (MD) and Centurion
631 Poultry Incorporated (GA) and incubated at 37°C in humidified incubators on their
632 sides. Embryos were incubated to reach desired Hamburger Hamilton (HH) stages
633 based on times provided therein (Hamburger and Hamilton, 1992).
634
635 **Morpholinos**
636 To reduce N-cadherin protein expression, a validated lissamine-tagged
637 translation-blocking morpholino antisense oligonucleotide (MO) against the *N-*
638 *cadherin* transcript was used (GeneTools, LLC) (Shiau and Bronner-Fraser, 2009),
639 with a sequence of 5'-GCGGCGTTCCCGCTATCCGGCACAT-3'. For some
640 control experiments, a 5 base pair mismatch N-cadherin control MO (N-cadherin
641 MM) was used (Shiau and Bronner-Fraser, 2009), with a sequence of 5'-
642 GCGcCcTTCCCcCTATgCcGCACAT-3' (altered base pairs in lowercase). Both
643 MOs were diluted with ultrapure water and 10% sucrose (in 1X phosphate-buffered
644 saline (PBS)) and used at a final concentration of 500 μM.
645
646 ***In ovo* unilateral placode electroporation**
647 To target trigeminal placode cells prior to their delamination, a unilateral
648 electroporation was performed at E1.75/HH10-11. The N-cadherin MO, N-
649 cadherin MM, or a combination of PiggyBacRFP, a genome incorporating vector
650 (Chen and LoTurco, 2012) (0.819 μg/μl), with PBase, its transposase (0.912 μg/μl),
651 was expelled on top of the ectoderm on one side of the embryo using a fine glass
652 needle. Next, a 30-gauge needle was used to puncture a small hole through the
653 vitelline membrane so that electrodes could lay vertically above and below the
654 ectoderm over which the MO/plasmid had been placed. Three, 9V pulses were
655 delivered over 50 ms at 200 ms intervals. After electroporation, eggs were resealed
656 with tape and parafilm and grown at 37°C to desired stages of interest. Due to the
657 inherent variations that arise during normal development, even when embryos are

658 staged identically, the contralateral side of the electroporated embryo was a more
659 appropriate control and was used for all *in vivo* studies. Embryos were screened
660 for successful MO electroporation based on the red fluorescence of the MO prior
661 to collection and use in subsequent assays.
662
663 **Sequential electroporation method**
664 To target both cell populations that contribute to the trigeminal ganglion, a
665 modified sequential electroporation (Halmi et al., 2022) was utilized. Briefly, a
666 unilateral neural tube co-electroporation was first performed on E1.5/HH9 using a
667 combination of PiggyBacGFP (0.819 µg/µl) and PBase (Wang et al., 2008) (0.912
668 µg/µl). Two, 15V pulses were delivered over 30 ms at 200 ms intervals. The
669 electroporated embryos were re-incubated until they reached E1.75/HH10-11, and
670 then the placode cells on the same side of the embryo were electroporated with
671 the N-cadherin MO, N-cadherin MM, or PiggyBacRFP in the same manner as
672 described above. After this second electroporation, eggs were resealed with tape
673 and parafilm and grown at 37°C to desired stages of interest.
674
675 **Immunostaining**
676 Electroporated embryos were collected at desired stages of interest and
677 fixed in 4% paraformaldehyde (PFA) overnight at 4°C with agitation. Following
678 fixation, embryos were washed 3 x 10 minutes in 1X PBS and stored in 1X PBS at
679 4°C until further processing. Primary antibodies used included Tubb3 (Abcam
680 ab78078, 1:500 for section, 1:250 for whole-mount), GFP (Abcam ab6662, 1:250),
681 RFP (Invitrogen MA5-15257, 1:250), TrkA (gift from Dr. Francis Lefcort, Montana
682 State University, 1:5000), TrkB (gift from Dr. Francis Lefcort, Montana State
683 University, 1:2500), cleaved caspase-3 (Cell Signaling Technology #9664, 1:100),
684 β-catenin (Santa Cruz Biotechnology sc-393501 1:100). Secondary antibodies
685 used at 1:250 included goat anti-rabbit IgG 488 (Invitrogen A211034), goat anti-
686 mouse IgG_1 594 (Invitrogen A21125), goat anti-mouse IgG_{2b} 647 (Invitrogen
687 A21242), goat anti-mouse 405 (Invitrogen A31553), and goat anti-mouse IgG_{2a}
688 555 or 647 (SouthernBiotech 1080-31 or 1080-32).

689 **Tissue sections:** Embryos were processed through an increasing sucrose
690 gradient (5% and 15% sucrose (Fisher) in 1X PBS) at 4°C either overnight or until
691 they sank to the bottom of the glass vials in which they were stored. Next, they
692 were processed through 7.5% gelatin (Sigma) in 15% sucrose and 20% gelatin in
693 1X PBS, both at 37°C, either overnight or until the embryos sank. Embryos were
694 embedded in 20% gelatin, flash-frozen using liquid nitrogen, and stored at -80°C
695 until ready for use. Embedded embryos were then cryo-sectioned at 12 μm on
696 charged slides (VWR, 48311-703). Slide-mounted tissue sections were stored at -
697 20°C until ready for use. For immunohistochemistry, slides were de-gelatinized by
698 incubation in 1X PBS at 42°C for 15-20 minutes. Following 3 x 5-minute washes in
699 1X PBS, the slides were blocked with 10% heat-treated sheep serum (Sigma,
700 HTSS) in 1X PBS + 0.1% Triton X-100 (Sigma, PBST) at room temperature for 1-
701 2 hours in a humidified chamber, then rinsed in PBST. Primary antibodies were
702 diluted in PBST + 5% HTSS, added to the slides, covered with a glass coverslip
703 (Fisher) to prevent sections from drying out, and incubated overnight at 4°C. The
704 following day, the coverslips were removed, and the slides were washed 4 x 30
705 minutes in PBST. Secondary antibodies were then diluted in PBST + 5% HTSS,
706 added to the slides, covered with a glass coverslip, and incubated overnight at
707 4°C. The next day, slides were again washed 4 x 30 minutes in PBST and mounted
708 with DAPI-fluoromount media (SouthernBiotech).
709 **Standard whole-mount immunohistochemistry:** Embryos were blocked
710 with 10% HTSS in PBST for 2 hours at room temperature. Following a rinse with
711 PBST, primary antibodies were diluted in PBST + 5% HTSS and incubated
712 overnight at 4°C with agitation. The following day, the embryos were washed 4 x
713 30 minutes in PBST. Secondary antibodies were diluted in PBST + 5% HTSS and
714 incubated overnight at 4°C with agitation. The next day, embryos were again
715 washed 4 x 30 minutes in PBST and stored in 1X PBS at 4°C until they were either
716 imaged or cleared (see below).
717 **Modified whole-mount immunohistochemistry for iDISCO clearing:** An
718 adapted protocol was used based on methods from (Renier et al., 2014). Fixed
719 embryos were washed twice for 1 hour in 1X PBS and were then taken through an

720 increasing methanol (MeOH, Pharmco) in 1X PBS gradient (50% (1 x 1 hour), 80%
721 (1 x 1 hour), 100% (2 x 1 hour)), before they were bleached overnight in 5% H_2O_2
722 (Sigma) in 20% DMSO (Fisher)/MeOH at 4°C. The next day, samples were taken
723 through the following series of washes: 2 x 1 hour in 100% MeOH, 2 x 1 hour in
724 20% DMSO/MeOH, 1 x 1 hour in 80% MeOH, 1 x 1 hour in 50% MeOH, 2 x 1 hour
725 in 1X PBS, and 2 x 1 hour in 1X PBS + 0.2% Triton X-100. Samples were incubated
726 overnight in 20% DMSO/0.3M glycine (Fisher) in 1X PBS + 0.2% Triton X-100 at
727 4°C. The next day, samples were blocked in 10% HTSS/10% DMSO/1X PBS +
728 0.2% Triton X-100 overnight at 4°C. Embryos were washed 2 x 1 hour in 0.2%
729 Tween-20 (Sigma) in 1X PBS with 10 µg/ml heparin (Fisher, PTwH) at room
730 temperature before primary antibodies were added and incubated for 72 hours at
731 4°C. Primary antibodies were diluted in 5% DMSO/5% HTSS/PTwH. Samples
732 were washed in PTwH for 24 hours before secondary antibodies were added
733 (diluted in the same manner as the primary antibodies), and samples were
734 incubated with secondary antibodies for 48 hours at 4°C. Samples were then
735 washed for 48 hours in PTwH before iDISCO clearing (see below).
736 **Explant immunocytochemistry:** Explant slides were washed once with 1X
737 PBS, followed by fixation in 4% PFA for 1 hour at room temperature with agitation.
738 Following fixation, slides were rinsed with 1X PBS and stored in 1X PBS at 4°C
739 until ready for immunocytochemistry. A hydrophobic perimeter was drawn around
740 the slides to prevent dehydration of tissue using an ImmEdge Pen (Vector
741 Laboratories), and explants were taken through blocking, primary antibody
742 incubation, and secondary antibody incubation in the absence of coverslips as
743 described in the tissue section methods. Slides were mounted with DAPI-
744 fluoromount media (SouthernBiotech) and covered with a glass coverslip.
745
746 **Tissue clearing**
747 As embryos progress through development and tissue structures
748 surrounding the trigeminal ganglion become more complex, visualization of the
749 trigeminal ganglion after whole-mount immunohistochemistry becomes
750 increasingly difficult. Therefore, clearing methods to render the tissues transparent

751 were performed. At early stages (up to E3.5/HH22), the FRUIT (Hou et al., 2015)
752 tissue clearing protocol was used, whereas later stages required iDISCO (Renier
753 et al., 2014) tissue clearing. With both protocols, MO fluorescence was quenched
754 during the clearing process.

755 **FRUIT:** Following the standard whole-mount immunohistochemistry
756 protocol, embryos were progressed through increasing concentrations of fructose
757 (35%, 40%, 60% and 80% w/v) in 8M urea (Sigma), 0.5% (v/v) alpha-thioglycerol
758 (Fisher) dissolved in ultrapure water ("FRUIT buffer") for a minimum of 8 hours, up
759 to 24 hours at room temperature, depending on the stage of the embryo. A sample
760 was only moved up to the next FRUIT buffer once it had visibly changed
761 transparency. The FRUIT cocktail, containing increasing concentrations of
762 fructose, was made by first dissolving fructose in ultrapure water at 37°C. Once
763 dissolved, the urea was added, and the solution was rocked at room temperature
764 until fully dissolved. Lastly, alpha-thioglycerol was added, and buffers were stored
765 at 4°C until use. Embryos were imaged in 60% or 80% FRUIT buffer (depending
766 on the stage of the embryo) in glass-bottomed petri dishes (MatTek P35G-1.5-20-
767 C). Typically, embryos up to E3/HH19 were imaged in 60% FRUIT while older
768 embryos were imaged in 80% FRUIT.

769 **iDISCO:** Following the modified whole-mount immunohistochemistry
770 protocol, embryos were washed in 1X PBS + 0.2% Triton X-100 for a minimum of
771 48 hours. Samples were incubated in 50% (v/v) tetrahydrofuran (Sigma, THF) in
772 water overnight in glass vials, making sure that over 90% of the vial was filled with
773 the solution. The following day, embryos were then incubated in 80% THF in water
774 for 1 hour, followed by 2 x 1 hour incubations in 100% THF. Next, samples were
775 incubated in 100% dichloromethane (Sigma) for 1-2 hours (or until they sank to the
776 bottom of the vial). Lastly, embryos were incubated in dibenzyl ether (Sigma, DBE)
777 overnight and imaged the following day in DBE. All steps, including embryo storage
778 in DBE, were performed at room temperature. iDISCO-cleared embryos were
779 imaged in a glass petri dish containing a custom chamber (Renier et al., 2014),
780 which was printed in Terrapin Works, part of the School of Engineering at the
781 University of Maryland.

782
783
784 **TUNEL assay**
785 To assess apoptosis (TUNEL), the *In Situ* Cell Death Detection Kit,
786 Fluorescein (Roche) was used according to manufacturer's instructions. Briefly,
787 following secondary antibody washes (4 x 30 minutes in PBST), slides were
788 washed once for 30 minutes in 1X PBS. Slides were re-fixed with 4% PFA for 20
789 minutes at room temperature, followed by one 30-minute wash in 1X PBS. The
790 TUNEL reaction mixture was added to the slides (75 µL per slide), and a glass
791 coverslip was placed over them. Slides were incubated in the dark for 1 hour at
792 37°C. Next, the coverslips were removed, and the slides were washed 3 x 5
793 minutes in 1X PBS. Lastly, slides were mounted with DAPI-fluoromount media
794 (SouthernBiotech).
795
796 **Trigeminal ganglion explant assay**
797 Wildtype E2/HH13-14 embryos were removed from eggs and stored on ice
798 in 1X PBS until dissections. Trigeminal ganglia were dissected on a sylgard-coated
799 dish by first bisecting the embryo and then carefully taking the area of the forming
800 trigeminal ganglion, making sure to exclude the eye and neural tube. Explants
801 were cultured on 2-well glass chamber slides (ThermoFisher) coated with Poly-L-
802 Lysine (0.01% PLL, Sigma) and fibronectin (0.01%, Sigma). To make the coated
803 slides, PLL was added to each chamber on the glass slides and incubated inside
804 a biosafety cabinet for 30 minutes at room temperature. The PLL was removed,
805 and slides were washed 3 times with water. Next, fibronectin (diluted in DMEM
806 media (ThermoFisher)) was added to each chamber and incubated at 37°C for a
807 minimum of 2 hours. The fibronectin solution was removed and slides were stored
808 at 4°C until needed (for up to one week). Explants were grown in DMEM media
809 supplemented with N2 (1%, ThermoFisher) and Penicillin/Streptomycin (1%,
810 Fisher). Explants for N-cadherin function-blocking antibody experiments (see
811 below) were grown in the supplemented DMEM media mentioned above.
812 Sequentially-labeled cells for N-cadherin MO- or MM-containing explant

813 experiments were grown in Neurobasal media (ThermoFisher) supplemented with
814 B27 (1%, ThermoFisher), N2 (0.5%, ThermoFisher), Glutamax (1%,
815 ThermoFisher), Penicillin/Streptomycin (1%, ThermoFisher), and with nerve
816 growth factor (ThermoFisher), brain-derived neurotrophic factor (Amgen), and
817 neurotrophin-3 (Amgen), all at 50 ng/ml.
818
819 **N-cadherin function-blocking antibody experiments**
820 After 24 hours of incubation, fresh media containing either an antibody to
821 block N-cadherin function, MNCD2 (anti-N-cadherin, Developmental Studies
822 Hybridoma Bank, 0.1 µg/ml), or a normal rat IgG control (Santa Cruz
823 Biotechnology, 1.6 µg/ml), replaced the initial explant plating media, and explants
824 were incubated overnight. The following morning, the slides were briefly rinsed
825 with 1X PBS and then fixed in 4% PFA for one hour at room temperature. The
826 explants were washed 3 times in 1X PBS and then processed for
827 immunocytochemistry.
828
829 **Immunoblotting**
830 E6.5/HH28-30 N-cadherin MO-electroporated and contralateral OpV lobes
831 from six embryos per replicate were dissected, pooled, and lysed in lysis buffer (50
832 mM Tris pH 7.5, 100 mM NaCl, 0.5% IGEPAL CA-630) supplemented with
833 cOmplete Protease Inhibitor Cocktail (Roche) and 1 mM PMSF for 30 minutes on
834 ice with periodic gentle vortexing. Lysates were then centrifuged at maximum *g* for
835 20 minutes at 4°C to separate fractions and the soluble protein fraction was then
836 quantified by Bradford assay (ThermoFisher). 12 µg of each sample was boiled at
837 99°C for 5 minutes in 4x reducing Laemmli sample buffer. Samples were separated
838 by 12% SDS-PAGE then transferred to PVDF membrane (ThermoFisher).
839 Membrane was blocked in 5% milk (in 1X PBS + 0.1% Tween-20) for 30 minutes
840 at room temperature followed by overnight incubation at 4°C with the following
841 primary antibodies diluted in blocking solution: Phospho-histone H3 (Sigma 06570,
842 1:500), N-cadherin (DSHB MNCD2, 1:100), and GAPDH (GeneTex GTX627408
843 1:1000). Membranes were washed 3 x 10 minutes in 1X PBS + 0.1% Tween-20

844 before incubation with secondary antibodies (species- and isotype-specific
845 horseradish peroxidase, Jackson ImmunoResearch) diluted in blocking solution for
846 1 hour at room temperature. Membranes were washed 3 x 10 minutes in 1X PBS
847 + 0.1% Tween-20 and antibody detection was performed using Supersignal West
848 Pico or Femto chemiluminescent substrates (ThermoFisher) and visualized using
849 a ChemiDox XRS system (Bio-Rad).
850
851 **Quantitative PCR**
852 Trigeminal ganglion explants in which placode cells were electroporated
853 with PiggyBacRFP plus PBase underwent rat IgG or anti-N-cadherin treatment (all
854 as described above). Explant cultures were pooled and lysed in RNA lysis buffer
855 and total RNA was extracted using the RNase Mini Kit (Qiagen). cDNAs were
856 synthesized using the SuperScript IV One-Step RT-PCR System (ThermoFisher)
857 according to manufacturer's instructions. Quantitative PCR was performed with
858 iTaq Universal SYBR Green Supermix (BioRad) according to manufacturer's
859 instructions. Equal amounts of cDNA for rat IgG- and anti-N-cadherin-treated
860 samples were used for quadruplicate reactions and mixed with SYBR Green
861 Supermix, and 750 nM of each primer (RFP or chick 18s rRNA). To validate results,
862 quantitative PCR was also performed on cDNA samples prepared in the absence
863 of reverse transcriptase and any template cDNA (no template control). *RFP* levels
864 were normalized against chick *18s* rRNA levels, as described previously
865 (Schiffmacher et al., 2016). Average normalized values of RFP were plotted as bar
866 graphs. Primer sequences are as follows: RFP Forward: (5'-
867 CTCCGAGGACGTCATCAA-3'), RFP Reverse: (5'-TTGGTCACCTTCAGCTTGG-
868 3'), chick *18s* rRNA Forward: (5'-TGTGCCGCTAGAGGTGAAATT-3'), and chick
869 18s rRNA Reverse: (5'-TGGCAAATGCTTTCGCTTT-3').
870
871 **Confocal imaging**
872 All images were acquired with the LSM Zeiss 800 confocal microscope (Carl
873 Zeiss Microscopy, Thornwood, NY, USA). Laser power, gain, and offset were kept
874 consistent for the different channels during all experiments where possible. Fiji

875 (NIH) (Schindelin et al., 2012) and Adobe Photoshop CC 2023 were used for
876 image processing. For whole-mount imaging with Z-stacks, all embryos were
877 imaged at a 5 μm interval. For sections, images of at least five serial transverse
878 sections were acquired and used for analysis. For all experiments, a minimum of
879 five replicates was obtained.
880
881 **Quantifications and statistical analyses**
882 All quantifications were done on Fiji and all graphs were generated using Prism
883 GraphPad Version 10.
884 **Area measurement:** Maximum intensity Z-projections were generated
885 through the trigeminal ganglion. The polygon tool was used to outline the perimeter
886 of Tubb3 signal, and area measurements were taken for the whole trigeminal
887 ganglion, the OpV lobe, and the MmV lobe. Individual area measurements for each
888 developmental stage grouping were averaged together and plotted to generate
889 graphs.
890 **Cell counting:** Cell counts were either performed manually or using the
891 Squassh (Rizk et al., 2014) plugin from the MOSAICsuite (Shivanandan et al.,
892 2013), as described (Halmi et al., 2022). The Tubb3 channel of each image was
893 used to crop the trigeminal ganglion, which was then used to crop the images for
894 the channel of interest. For Squassh, segmentation parameters were kept uniform
895 for all images and run as a batch function. The quality of image segmentation was
896 confirmed visually, and adjustments were made as necessary. The number of
897 puncta/cells was calculated per image and averaged to obtain a mean number per
898 replicate, which was then divided by the average area of the trigeminal ganglion to
899 adjust for size differences. Individual averages for each developmental stage
900 grouping were plotted to generate graphs.
901 **Nerve branching:** Z-stack images of the OpV branch of the trigeminal
902 nerve were analyzed using custom ImageJ Macro language (IJM) scripts (available
903 upon request). Maximum intensity Z-projections were generated and input into the
904 ImageJ macro. Signal profiles were obtained via successive vertical line selections
905 using *getProfile()* at 30 μm intervals. The number of terminal nerve branches

906 present at increasing distances from the starting point were exported and
907 calculated in R (R core team, Vienna, Austria, 2021, scripts available upon
908 request). Data were aligned to ensure consistent starting points for each replicate,
909 and the mean number of nerve branches was plotted to generate graphs.

910 **Nerve width:** Nerve width measurements for both the lateral and medial
911 nasal nerves were generated using maximum intensity Z-projections and the
912 straight line tool. The width of individual OpV nerve divisions (prior to extensive
913 branching within the target tissue) was measured based on the Tubb3 signal for
914 each embryo. Widths for N-cadherin MO-treated embryos and their contralateral
915 control sides were averaged and plotted to generate graphs.

916 **Innervation area:** Maximum intensity Z-projections were used to generate
917 innervation area measurements for both the lateral and medial nasal nerves. The
918 polygon tool was used to draw a border around the Tubb3 signal in the target
919 tissues where terminal nerve branching occurred. Area measurements for N-
920 cadherin MO-treated embryos and their contralateral control sides were averaged
921 and plotted to generate graphs.

922 **Intersection analysis following treatment with anti-N-cadherin**:
923 Background was removed and the ridge-detection plug-in (Steger, 1998) was used
924 to highlight axonal outgrowth and to quantify axon length from explant images.
925 Using the detected segment binary images and the concentric circle plugin, 20
926 concentric circles were overlayed on the explant, centered at the middle. The
927 number of axonal intersections at each successive ring of increasing diameter was
928 counted and plotted to generate graphs.

929 **RFP-labeled placode cell analysis:** Background was eliminated from
930 explant images of the Tubb3 channel and the polygon tool was used to isolate the
931 core of the explant from its associated axonal projections. The fluorescent intensity
932 of RFP signal was collected for both the axonal projections and the core of the
933 explants. The mean axonal signal was divided by the mean core signal to generate
934 a ratio. Ratios for individual treatments were averaged and compared between
935 conditions.

936 **Simple neurite tracer analysis:** Z-stacks of GFP-positive neural crest-
937 derived neurons were analyzed using the simple neurite tracer plugin (Arshadi et
938 al., 2021; Ferreira et al., 2014). Primary neurites were traced from the cell body
939 through the entire Z-stack. Neurites extending from primary neurites were added
940 as branch points and termed secondary neurites. Any neurite branching off
941 secondary neurites was marked as a tertiary neurite. The mean number and mean
942 length of primary, secondary, and tertiary neurites were plotted to generate graphs.
943 **Immunoblot band intensity:** Immunoblot images were processed with the
944 Analyze Gel function. Equal boxes were drawn around the lanes of interest using
945 the rectangle tool, and band intensities were plotted as peaks of signal. The line
946 tool was used to isolate peaks and remove background, measuring the area under
947 the peak to quantify band intensity for each protein. Phospho-histone H3 and N-
948 cadherin were normalized against GAPDH and plotted to generate graphs.
949 **β-catenin analysis:** Z-stack images of sequentially-electroporated
950 explants were processed using custom ImageJ Macro language (IJM) scripts
951 (available upon request). GFP-positive neurons were identified over each slice
952 using thresholding. The area of each identified cell was calculated using the
953 analyze particles tool, and the mean β-catenin signal was quantified from the
954 overlapping GFP signal in the Z-stacks. Slices with insufficient β-catenin staining
955 were excluded. Mean β-catenin signal was plotted to generate graphs.
956
957

ACKNOWLEDGMENTS

The authors would like to thank the National Institute of Dental and Craniofacial Research (R01DE024217) and the University of Maryland Graduate School for financially supporting this research. Additionally, we would like to thank Ms. Zoe Davidson and Ms. Reagan Armstrong for their technical assistance. All schematics were created with Biorender.com.

COMPETING INTERESTS

No competing interests declared.

DATA AND RESOURCE AVAILABILITY

All relevant data can be found within this article and the supplementary information.

REFERENCES

Arshadi, C., Günther, U., Eddison, M., Harrington, K.I.S., Ferreira, T.A., 2021. SNT: a unifying toolbox for quantification of neuronal anatomy. Nat Methods 18, 374–377. https://doi.org/10.1038/s41592-021-01105-7

Basu, R., Duan, X., Taylor, M.R., Martin, E.A., Muralidhar, S., Wang, Y., Gangi-Wellman, L., Das, S.C., Yamagata, M., et al. 2017. Heterophilic Type II Cadherins Are Required for High-Magnitude Synaptic Potentiation in the Hippocampus. Neuron 96, 160-176.e8. https://doi.org/10.1016/j.neuron.2017.09.009

Bate, C.M., 1976. Pioneer neurones in an insect embryo. Nature 260, 54–56. https://doi.org/10.1038/260054a0

Begbie, J., 2002. Early Steps in the Production of Sensory Neurons by the Neurogenic Placodes. Molecular and Cellular Neuroscience 21, 502–511. https://doi.org/10.1006/mcne.2002.1197

Benson, D.L., Tanaka, H., 1998. N-Cadherin Redistribution during Synaptogenesis in Hippocampal Neurons. J. Neurosci. 18, 6892–6904. https://doi.org/10.1523/JNEUROSCI.18-17-06892.1998

Bill, B.R., Petzold, A.M., Clark, K.J., Schimmenti, L.A., Ekker, S.C., 2009. A Primer for Morpholino Use in Zebrafish. Zebrafish 6, 69–77. https://doi.org/10.1089/zeb.2008.0555

Bixby, J.L., Zhang, R., 1990. Purified N-cadherin is a potent substrate for the rapid induction of neurite outgrowth. J Cell Biol 110, 1253–1260. https://doi.org/10.1083/jcb.110.4.1253

Bronner-Fraser, M., Wolf, J.J., Murray, B.A., 1992. Effects of antibodies against N-cadherin and N-CAM on the cranial neural crest and neural tube. Developmental Biology 153, 291–301. https://doi.org/10.1016/0012-1606(92)90114-V

Chen, F., LoTurco, J., 2012. A method for stable transgenesis of radial glia lineage in rat neocortex by piggyBac mediated transposition. J Neurosci Methods 207, 172–180. https://doi.org/10.1016/j.jneumeth.2012.03.016

Chiasson-MacKenzie, C., McClatchey, A.I., 2018. Cell–Cell Contact and Receptor Tyrosine Kinase Signaling. Cold Spring Harb Perspect Biol 10, a029215. https://doi.org/10.1101/cshperspect.a029215

Clarke, A., McQueen, P.G., Fang, H.Y., Kannan, R., Wang, V., McCreedy, E., Buckley, T., Johannessen, E., Wincovitch, S., Giniger, E., 2020. Dynamic morphogenesis of a pioneer axon in *Drosophila* and its regulation by Abl tyrosine kinase. MBoC 31, 452–465. https://doi.org/10.1091/mbc.E19-10-0563

Dady, A., Blavet, C., Duband, J.-L., 2012. Timing and kinetics of E- to N-cadherin switch during neurulation in the avian embryo. Dev. Dyn. 241, 1333–1349. https://doi.org/10.1002/dvdy.23813

D'Amico-Martel, A., Noden, D.M., 1980. An autoradiographic analysis of the development of the chick trigeminal ganglion. J Embryol Exp Morphol 55, 167–182.

D'Amico-Martel, A., Noden, D.M., 1983. Contributions of placodal and neural crest cells to avian cranial peripheral ganglia. Am. J. Anat. 166, 445–468. https://doi.org/10.1002/aja.1001660406

Eisen, J.S., Myers, P.Z., Westerfield, M., 1986. Pathway selection by growth cones of identified motoneurones in live zebra fish embryos. Nature 320, 269–271. https://doi.org/10.1038/320269a0

Ferreira, T.A., Blackman, A.V., Oyrer, J., Jayabal, S., Chung, A.J., Watt, A.J., Sjöström, P.J., Van Meyel, D.J., 2014. Neuronal morphometry directly from bitmap images. Nat Methods 11, 982–984. https://doi.org/10.1038/nmeth.3125

1052 Gärtner, A., Fornasiero, E.F., Munck, S., Vennekens, K., Seuntjens, E., Huttner, W.B.,
1053 Valtorta, F., Dotti, C.G., 2012. N-cadherin specifies first asymmetry in developing
1054 neurons. EMBO J 31, 1893–1903. https://doi.org/10.1038/emboj.2012.41
1055 Ghosh, A., Antonini, A., McConnell, S.K., Shatz, C.J., 1990. Requirement for subplate
1056 neurons in the formation of thalamocortical connections. Nature 347, 179–181.
1057 https://doi.org/10.1038/347179a0
1058 Gong, Q., Shipley, M.T., 1995. Evidence that pioneer olfactory axons regulate
1059 telencephalon cell cycle kinetics to induce the formation of the olfactory bulb.
1060 Neuron 14, 91–101. https://doi.org/10.1016/0896-6273(95)90243-0
1061 Graham, A., Shimeld, S.M., 2013. The origin and evolution of the ectodermal placodes.
1062 Journal of Anatomy 222, 32–40. https://doi.org/10.1111/j.1469-7580.2012.01506.x
1063 Halbleib, J.M., Nelson, W.J., 2006. Cadherins in development: cell adhesion, sorting, and
1064 tissue morphogenesis. Genes Dev. 20, 3199–3214.
1065 https://doi.org/10.1101/gad.1486806
1066 Halmi, C.A., Wu, C.-Y., Taneyhill, L.A., 2022. Neural crest cell-placodal neuron
1067 interactions are mediated by Cadherin-7 and N-cadherin during early chick
1068 trigeminal ganglion assembly. F1000Res 11, 741.
1069 https://doi.org/10.12688/f1000research.122686.2
1070 Hamburger, V., 1961. Experimental analysis of the dual origin of the trigeminal ganglion
1071 in the chick embryo. J. Exp. Zool. 148, 91–123.
1072 https://doi.org/10.1002/jez.1401480202
1073 Hamburger, V., Hamilton, H.L., 1992. A series of normal stages in the development of the
1074 chick embryo. Developmental Dynamics 195, 231–272.
1075 https://doi.org/10.1002/aja.1001950404
1076 Hansen, S.M., Berezin, V., Bock, E., 2008. Signaling mechanisms of neurite outgrowth
1077 induced by the cell adhesion molecules NCAM and N-Cadherin. Cell. Mol. Life Sci.
1078 65, 3809–3821. https://doi.org/10.1007/s00018-008-8290-0
1079 Hatta, K., Takeichi, M., 1986. Expression of N-cadherin adhesion molecules associated
1080 with early morphogenetic events in chick development. Nature 320, 447–449.
1081 https://doi.org/10.1038/320447a0
1082 Heimer, L., 1983. Cranial Nerves, in: The Human Brain and Spinal Cord. Springer US,
1083 New York, NY, pp. 237–260. https://doi.org/10.1007/978-1-4684-0150-9_18
1084 Hidalgo, A., Brand, A.H., 1997. Targeted neuronal ablation: the role of pioneer neurons in
1085 guidance and fasciculation in the CNS of *Drosophila*. Development 124, 3253–
1086 3262. https://doi.org/10.1242/dev.124.17.3253
1087 Higashiyama, H., Kuratani, S., 2014. On the maxillary nerve: The Maxillary Nerve in
1088 Vertebrates. Journal of Morphology 275, 17–38.
1089 https://doi.org/10.1002/jmor.20193
1090 Hou, B., Zhang, D., Zhao, S., Wei, M., Yang, Z., Wang, S., Wang, J., Zhang, X., Liu, B.,
1091 Fan, L., et al. 2015. Scalable and DiI-compatible optical clearance of the
1092 mammalian brain. Front Neuroanat 9, 19.
1093 https://doi.org/10.3389/fnana.2015.00019
1094 Inuzuka, H., Redies, C., Takeichi, M., 1991. Differential expression of R- and N-cadherin
1095 in neural and mesodermal tissues during early chicken development. Development
1096 113, 959–967. https://doi.org/10.1242/dev.113.3.959
1097 Itoh, K., Ozaki, M., Stevens, B., Fields, R.D., 1997. Activity-dependent regulation of N-
1098 cadherin in DRG neurons: differential regulation of N-cadherin, NCAM, and L1 by
1099 distinct patterns of action potentials. J Neurobiol 33, 735–748.
1100 https://doi.org/10.1002/(sici)1097-4695(19971120)33:6<735::aid-neu3>3.0.co;2-a
1101 Jontes, J.D., 2018. The Cadherin Superfamily in Neural Circuit Assembly. Cold Spring
1102 Harb Perspect Biol 10, a029306. https://doi.org/10.1101/cshperspect.a029306

1103 Klose, M., Bentley, D., 1989. Transient pioneer neurons are essential for formation of an
1104 embryonic peripheral nerve. Science 245, 982–984.
1105 https://doi.org/10.1126/science.2772651
1106 Lassiter, R.N.T., Stark, M.R., Zhao, T., Zhou, C.J., 2014. Signaling mechanisms
1107 controlling cranial placode neurogenesis and delamination. Developmental
1108 Biology 389, 39–49. https://doi.org/10.1016/j.ydbio.2013.11.025
1109 Lin, D.M., Auld, V.J., Goodman, C.S., 1995. Targeted neuronal cell ablation in the
1110 drosophila embryo: Pathfinding by follower growth cones in the absence of
1111 pioneers. Neuron 14, 707–715. https://doi.org/10.1016/0896-6273(95)90215-5
1112 Lu, Y., Lin, C., Wang, X., 2009. PiggyBac transgenic strategies in the developing chicken
1113 spinal cord. Nucleic Acids Research 37, e141–e141.
1114 https://doi.org/10.1093/nar/gkp686
1115 Lumsden, A., Sprawson, N., Graham, A., 1991. Segmental origin and migration of neural
1116 crest cells in the hindbrain region of the chick embryo. Development 113, 1281–
1117 1291. https://doi.org/10.1242/dev.113.4.1281
1118 Macdonald, J., Taylor, L., Sherman, A., Kawakami, K., Takahashi, Y., Sang, H.M.,
1119 McGrew, M.J., 2012. Efficient genetic modification and germ-line transmission of
1120 primordial germ cells using piggyBac and Tol2 transposons. Proc. Natl. Acad. Sci.
1121 U.S.A. 109. https://doi.org/10.1073/pnas.1118715109
1122 Masai, I., Lele, Z., Yamaguchi, M., Komori, A., Nakata, A., Nishiwaki, Y., Wada, H.,
1123 Tanaka, H., Nojima, Y., Hammerschmidt, M., et al. 2003. N-cadherin mediates
1124 retinal lamination, maintenance of forebrain compartments and patterning of retinal
1125 neurites. Development 130, 2479–2494. https://doi.org/10.1242/dev.00465
1126 McCabe, K.L., Sechrist, J.W., Bronner-Fraser, M., 2009. Birth of ophthalmic trigeminal
1127 neurons initiates early in the placodal ectoderm. J of Comparative Neurology 514,
1128 161–173. https://doi.org/10.1002/cne.22004
1129 Miyamoto, Y., Sakane, F., Hashimoto, K., 2015. N-cadherin-based adherens junction
1130 regulates the maintenance, proliferation, and differentiation of neural progenitor
1131 cells during development. Cell Adhesion & Migration 9, 183–192.
1132 https://doi.org/10.1080/19336918.2015.1005466
1133 Moody, S.A., Heaton, M.B., 1983. Developmental relationships between trigeminal
1134 ganglia and trigeminal motoneurons in chick embryos. I. Ganglion development is
1135 necessary for motoneuron migration. J of Comparative Neurology 213, 327–343.
1136 https://doi.org/10.1002/cne.902130308
1137 Moody, S.A., Quigg, M.S., Frankfurter, A., 1989. Development of the peripheral trigeminal
1138 system in the chick revealed by an isotype-specific anti-beta-tubulin monoclonal
1139 antibody. J of Comparative Neurology 279, 567–580.
1140 https://doi.org/10.1002/cne.902790406
1141 Nakagawa, S., Takeichi, M., 1997. N-cadherin is crucial for heart formation in the chick
1142 embryo. Dev Growth Differ 39, 451–455. https://doi.org/10.1046/j.1440-
1143 169X.1997.t01-3-00006.x
1144 Nguyen, T., Mège, R.M., 2016. N-Cadherin and Fibroblast Growth Factor Receptors
1145 crosstalk in the control of developmental and cancer cell migrations. European
1146 Journal of Cell Biology 95, 415–426. https://doi.org/10.1016/j.ejcb.2016.05.002
1147 Niessen, C.M., Leckband, D., Yap, A.S., 2011. Tissue organization by cadherin adhesion
1148 molecules: dynamic molecular and cellular mechanisms of morphogenetic
1149 regulation. Physiol Rev 91, 691–731. https://doi.org/10.1152/physrev.00004.2010
1150 Noden, D.M., 1973. The migratory behavior of neural crest cells. Symp Oral Sens Percept
1151 9–36.

1152 Radice, G.L., 2013. N-Cadherin-Mediated Adhesion and Signaling from Development to
1153 Disease, in: Progress in Molecular Biology and Translational Science. Elsevier, pp.
1154 263–289. https://doi.org/10.1016/B978-0-12-394311-8.00012-1
1155 Redies, C., Inuzuka, H., Takeichi, M., 1992. Restricted expression of N- and R-cadherin
1156 on neurites of the developing chicken CNS. J Neurosci 12, 3525–3534.
1157 https://doi.org/10.1523/JNEUROSCI.12-09-03525.1992
1158 Reis, S.A., Thompson, M.N., Lee, J.-M., Fossale, E., Kim, H.-H., Liao, J.K., Moskowitz,
1159 M.A., Shaw, S.Y., Dong, L., Haggarty, S.J., et al. 2011. Striatal neurons expressing
1160 full-length mutant huntingtin exhibit decreased N-cadherin and altered
1161 neuritogenesis. Human Molecular Genetics 20, 2344–2355.
1162 https://doi.org/10.1093/hmg/ddr127
1163 Renier, N., Wu, Z., Simon, D.J., Yang, J., Ariel, P., Tessier-Lavigne, M., 2014. iDISCO: A
1164 Simple, Rapid Method to Immunolabel Large Tissue Samples for Volume Imaging.
1165 Cell 159, 896–910. https://doi.org/10.1016/j.cell.2014.10.010
1166 Riehl, R., Johnson, K., Bradley, R., Grunwald, G.B., Cornel, E., Lilienbaum, A., Holt, C.E.,
1167 1996. Cadherin Function Is Required for Axon Outgrowth in Retinal Ganglion Cells
1168 In Vivo. Neuron 17, 837–848. https://doi.org/10.1016/S0896-6273(00)80216-0
1169 Rizk, A., Paul, G., Incardona, P., Bugarski, M., Mansouri, M., Niemann, A., Ziegler, U.,
1170 Berger, P., Sbalzarini, I.F., 2014. Segmentation and quantification of subcellular
1171 structures in fluorescence microscopy images using Squassh. Nat Protoc 9, 586–
1172 596. https://doi.org/10.1038/nprot.2014.037
1173 Sainath, R., Gallo, G., 2015. Cytoskeletal and signaling mechanisms of neurite formation.
1174 Cell Tissue Res 359, 267–278. https://doi.org/10.1007/s00441-014-1955-0
1175 Schiffmacher, A.T., Xie, V., Taneyhill, L.A., 2016. Cadherin-6B proteolysis promotes the
1176 neural crest cell epithelial-to-mesenchymal transition through transcriptional
1177 regulation. Journal of Cell Biology 215, 735–747.
1178 https://doi.org/10.1083/jcb.201604006
1179 Schindelin, J., Arganda-Carreras, I., Frise, E., Kaynig, V., Longair, M., Pietzsch, T.,
1180 Preibisch, S., Rueden, C., Saalfeld, S., Schmid, B., et al. 2012. Fiji: an open-source
1181 platform for biological-image analysis. Nature Methods 9, 676–682.
1182 https://doi.org/10.1038/nmeth.2019
1183 Shiau, C.E., Bronner-Fraser, M., 2009. N-cadherin acts in concert with Slit1-Robo2
1184 signaling in regulating aggregation of placode-derived cranial sensory neurons.
1185 Development 136, 4155–4164. https://doi.org/10.1242/dev.034355
1186 Shiau, C.E., Das, R.M., Storey, K.G., 2011. An effective assay for high cellular resolution
1187 time-lapse imaging of sensory placode formation and morphogenesis. BMC
1188 Neurosci 12, 37. https://doi.org/10.1186/1471-2202-12-37
1189 Shiau, C.E., Lwigale, P.Y., Das, R.M., Wilson, S.A., Bronner-Fraser, M., 2008. Robo2-
1190 Slit1 dependent cell-cell interactions mediate assembly of the trigeminal ganglion.
1191 Nat Neurosci 11, 269–276. https://doi.org/10.1038/nn2051
1192 Shikanai, M., Nishimura, Y.V., Sakurai, M., Nabeshima, Y., Yuzaki, M., Kawauchi, T.,
1193 2018. Caveolin-1 Promotes Early Neuronal Maturation via Caveolae-Independent
1194 Trafficking of N-Cadherin and L1. iScience 7, 53–67.
1195 https://doi.org/10.1016/j.isci.2018.08.014
1196 Shivanandan, A., Radenovic, A., Sbalzarini, I.F., 2013. MosaicIA: an ImageJ/Fiji plugin for
1197 spatial pattern and interaction analysis. BMC Bioinformatics 14, 349.
1198 https://doi.org/10.1186/1471-2105-14-349
1199 Stainier, D.Y., Gilbert, W., 1990. Pioneer neurons in the mouse trigeminal sensory system.
1200 Proc Natl Acad Sci U S A 87, 923–927. https://doi.org/10.1073/pnas.87.3.923

Stark, M.R., Sechrist, J., Bronner-Fraser, M., Marcelle, C., 1997. Neural tube-ectoderm interactions are required for trigeminal placode formation. Development 124, 4287–4295. https://doi.org/10.1242/dev.124.21.4287

Steger, C., 1998. An unbiased detector of curvilinear structures. IEEE Trans. Pattern Anal. Machine Intell. 20, 113–125. https://doi.org/10.1109/34.659930

Steventon, B., Mayor, R., Streit, A., 2014. Neural crest and placode interaction during the development of the cranial sensory system. Developmental Biology 389, 28–38. https://doi.org/10.1016/j.ydbio.2014.01.021

Straub, B.K., Rickelt, S., Zimbelmann, R., Grund, C., Kuhn, C., Iken, M., Ott, M., Schirmacher, P., Franke, W.W., 2011. E–N-cadherin heterodimers define novel adherens junctions connecting endoderm-derived cells. The Journal of Cell Biology 195, 873–887. https://doi.org/10.1083/jcb.201106023

Tan, Z.-J., Peng, Y., Song, H.-L., Zheng, J.-J., Yu, X., 2010. N-cadherin-dependent neuron–neuron interaction is required for the maintenance of activity-induced dendrite growth. Proc. Natl. Acad. Sci. U.S.A. 107, 9873–9878. https://doi.org/10.1073/pnas.1003480107

Theveneau, E., Steventon, B., Scarpa, E., Garcia, S., Trepat, X., Streit, A., Mayor, R., 2013. Chase-and-run between adjacent cell populations promotes directional collective migration. Nat Cell Biol 15, 763–772. https://doi.org/10.1038/ncb2772

Vermeiren, S., Bellefroid, E.J., Desiderio, S., 2020. Vertebrate Sensory Ganglia: Common and Divergent Features of the Transcriptional Programs Generating Their Functional Specialization. Front Cell Dev Biol 8, 587699. https://doi.org/10.3389/fcell.2020.587699

Wang, W., Lin, C., Lu, D., Ning, Z., Cox, T., Melvin, D., Wang, X., Bradley, A., Liu, P., 2008. Chromosomal transposition of *PiggyBac* in mouse embryonic stem cells. Proc. Natl. Acad. Sci. U.S.A. 105, 9290–9295. https://doi.org/10.1073/pnas.0801017105

Wanner, S.J., Prince, V.E., 2013. Axon tracts guide zebrafish facial branchiomotor neuron migration through the hindbrain. Development 140, 906–915. https://doi.org/10.1242/dev.087148

Williams, R., Bäckström, A., Kullander, K., Hallböök, F., Ebendal, T., 1995. Developmentally Regulated Expression of mRNA for Neurotrophin High-Affinity (*trk*) Receptors within Chick Trigeminal Sensory Neurons. Eur J of Neuroscience 7, 116–128. https://doi.org/10.1111/j.1460-9568.1995.tb01026.x

Wu, C., Taneyhill, L.A., 2019. Cadherin-7 mediates proper neural crest cell–placodal neuron interactions during trigeminal ganglion assembly. genesis 57, e23264. https://doi.org/10.1002/dvg.23264

1240 ## FIGURE LEGENDS

1241 **Figure 1. Knockdown of N-cadherin in placode cells disrupts trigeminal ganglion**
1242 **development.** (A-E') Representative images of the trigeminal ganglion (contralateral control and
1243 N-cadherin MO-electroporated side) after Tubb3 immunostaining (E2.5/HH16-18: A-A' (n=10),
1244 E3.5/HH19-22: B-B' (n=10), E4.5/HH23-25: C-C' (n=14), E5.5/HH26-27: D-D' (n=13), E6.5/HH28-
1245 30: E-E' (n=6)). Arrowheads highlight reductions in OpV lobe size in N-cadherin MO samples
1246 compared to controls. Scale bar in (A) is 250 μm and applies to (A'-B'); scale bar in (C) is 250 μm
1247 and applies to (C'-E'). (F-H) Mean area ± SEM of whole trigeminal ganglia (F), OpV branch (G),
1248 and MmV/MxV branch (H) for contralateral and N-cadherin MO sides of embryos. Statistical
1249 significance was determined via paired t-tests and Wilcoxon signed-rank test. (*) $p<0.05$, (**)
1250 $p<0.01$, (***) $p<0.001$, (****) $p<0.0001$. Abbreviations: TG: trigeminal ganglion; OpV: ophthalmic;
1251 MmV: maxillomandibular; MxV: maxillary; MnV: mandibular; ns: not significant.
1252

1253 **Figure 2. N-cadherin depletion from placode cells negatively impacts outgrowth and target**
1254 **tissue innervation for OpV nerve branches.** (A, B, F, G) Representative images of the lateral (A,
1255 B) and medial (F, G) nasal nerves (contralateral control and N-cadherin MO-electroporated side)
1256 after Tubb3 immunostaining (A, B: E4.5/HH23-25 (n=12); F, G: E5.5/HH26-27 (n=13)). Scale bars
1257 in (A) and (F) are 250 μm and apply to (B) and (G), respectively. (C, H) Mean ± SEM of terminal
1258 nerve endings. Significant distances in (C) are observed at 420, 450, 480, and 530 μm (*); 300 and
1259 570 μm (**); and 330, 360, and 390 μm (***). No significant differences were observed in (H). (D, I)
1260 Mean nerve width ± SEM. (E, J) Mean innervation area ± SEM. Statistical significance was
1261 determined via paired t-tests (C-E, H-J), with adjustments made for multiple comparisons (C, H).
1262 (*) $p<0.05$, (**) $p<0.01$, (***) $p<0.001$.
1263

1264 **Figure 3. Morphological changes in the trigeminal ganglion after N-cadherin knockdown in**
1265 **placode cells are in part due to increased cell death** (A-B') Transverse sections through the
1266 OpV lobe (contralateral control and N-cadherin MO-electroporated side) from representative
1267 E2.25/HH16 embryos with Tubb3 immunostaining and TUNEL staining. Scale bar in (A) is 50 μm
1268 and applies to all images. (C) Five serial sections per embryo from stage groupings E1.5/HH13-16
1269 (n=6), E2.5/HH16-18 (n=6), E3.5/HH19-22 (n=8), and E4.5/HH23-25 (n=11) were imaged and used
1270 for analysis. Arrowheads in (A', B') mark TUNEL puncta. Statistical significance was determined
1271 via paired t-tests and Wilcoxon signed-rank test. (*) $p<0.05$. Abbreviations: e: ectoderm; ns: not
1272 significant.
1273

1274 **Figure 4. N-cadherin depletion from placode cells decreases neurite complexity in neural-**
1275 **crest derived neurons.** (A) Schematic of sequential electroporation explant culture technique. (B-
1276 E) Representative maximum intensity Z-projections of GFP-labeled neural crest-derived neurons

1277 after placodal electroporation with N-cadherin MM (B-B', control, (n=13)) or N-cadherin MO (D-D',
1278 (n=17)) from trigeminal ganglion explants following GFP and Tubb3 immunostaining, and neurite-
1279 traced images (C, E). Arrowheads and asterisks denote examples of primary and secondary
1280 neurites, respectively. Scale bar in (B) is 50 μm and applies to (B', D-D'); scale bar in (C) is 10 μm
1281 and applies to (E). Mean number (F) and length (G) ± SEM of GFP-positive neural crest-derived
1282 neurites after N-cadherin MM or N-cadherin MO electroporation. (H-I) Representative maximum Z-
1283 projections of GFP-labeled neural crest-derived neurons after placodal electroporation with N-
1284 cadherin MM (H, n=3) or N-cadherin MO (I, n=4) from trigeminal ganglion explants following GFP
1285 and β-catenin immunostaining. Arrowheads indicate colocalization of GFP and β-catenin staining.
1286 Scale bar in (H) is 10 μm and applies to (I). (J) Mean β-catenin signal intensity ± SEM in GFP-
1287 positive neural crest-derived neurons. Statistical significance was determined via unpaired t-tests
1288 and Mann-Whitney tests (F-G). (*) $p<0.05$, (**) $p<0.01$, (****) $p<0.0001$. Abbreviations: ns: not
1289 significant.
1290
1291 **Figure 5. Blocking N-cadherin-mediated adhesion reduces trigeminal neuron axon**
1292 **outgrowth.** (A) Schematic of N-cadherin function-blocking assay. (B-D") Workflow for *in vitro*
1293 analyses. (B, C, D) Representative images of wildtype trigeminal ganglion explants after 24 hours
1294 (hr) of incubation and fixation (pre-treatment control explants (n=31)), or post-treatment with either
1295 rat IgG (n=7) or anti-N-cadherin (n=9) antibody, followed by Tubb3 immunostaining. Scale bar in
1296 (B) is 1 mm and applies to (C, D). (B', C', D') Binary images generated after ridge detection
1297 processing on Fiji for pre-treatment, anti-N-cadherin-treated, or rat IgG-treated explants,
1298 respectively. Dotted lines indicate perimeter of explanted tissue cropped during processing. (B",
1299 C", D") Processed images overlaid with concentric circle function to count the number of axonal
1300 intersections at increasing intervals of 175 μm. (E) Mean signal intensity for explant outgrowth ±
1301 SEM. (F) Mean number of axonal intersections ± SEM. Significant differences between pre-
1302 treatment control explants and anti-N-cadherin-treated explants are observed at 525 μm (*) and
1303 175, 350, 875, 1225, and 1400 μm (**). Significant differences between pre-treatment controls and
1304 rat IgG-treated explants are observed at 1750 μm (*), 1575 μm (**), and 175-1400 μm (****).
1305 Significant differences between anti-N-cadherin- and rat IgG-treated explants are observed at 175,
1306 350, and 700 μm (*) and 525 μm (**). (G) Mean segment length ± SEM. (H) Violin plots of segment
1307 lengths for pre-treatment, anti-N-cadherin-treated, and rat IgG-treated explants. Solid black lines
1308 indicate median and dotted black lines indicate interquartile range. Statistical significance was
1309 determined via unpaired t-tests and Mann-Whitney tests (E-G) with adjustments made for multiple
1310 comparisons (F). (*) $p<0.05$, (**) $p<0.01$, (***) $p<0.001$, (****) $p<0.0001$.
1311
1312 **Figure 6. The majority of placodal neurons rely on N-cadherin for axon outgrowth.** (A-D")
1313 Representative images of trigeminal explant cultures with RFP-labeled placodal neurons after rat

1314 IgG (A-B” (n=8)) or anti-N-cadherin (C-D” (n=8)) treatment and RFP and Tubb3 immunostaining.
1315 Boxes in (A) and (C) indicate higher magnification images in (B-B”), and (D-D”), respectively. Dotted
1316 lines in (A) and (C) indicate the perimeter of the explanted tissue. Scale bar in (A) is 500 μm and
1317 applies to (C); scale bar in (B) is 100 μm and applies to (B’-B”, D-D”). (E) Mean signal intensity for
1318 Tubb3 and RFP ± SEM. (F) Quantitative PCR for *RFP* normalized against chick *18s* rRNA of rat
1319 IgG- and anti-N-cadherin-treated explants (n=3). (G) Trigeminal ganglion explant culture
1320 schematic, with cores (inside the explant) and axons (outside the explant) comprising the explant
1321 culture. (H) Ratio of RFP signal found within axons and cores ± SEM. Statistical significance was
1322 determined via unpaired t-tests and Mann-Whitney tests (E, F, H) (*) $p<0.05$, (***) $p<0.001$.
1323
1324 **Figure 7: Blocking N-cadherin-mediated adhesion reduces neurite complexity in neural**
1325 **crest-derived neurons.** (A) Schematic of N-cadherin function blocking assay after labeling neural
1326 crest-derived neurons with PiggyBacGFP. (B-C) Representative images of trigeminal explant
1327 cultures with GFP-labeled neural crest-derived neurons after control rat IgG (B, (n=7)) or anti-N-
1328 cadherin (C, (n=7)) treatment, GFP immunostaining, and neurite traced images (B’, C’).
1329 Arrowheads and asterisks denote examples of primary and secondary neurites, respectively. Scale
1330 bar in (B) is 50 μm and applies to (C); scale bar in (B’) is 25 μm and applies to (C’). Mean number
1331 (D) and length (E) ± SEM of GFP-positive neural crest-derived neurites after rat IgG or anti-N-
1332 cadherin treatment. Statistical significance was determined via unpaired t-tests and Mann-Whitney
1333 tests (D-E). (*) $p<0.05$, (**) $p<0.01$. Abbreviations: ns: not significant.
1334

1335 **SUPPLEMENTAL FIGURE LEGENDS**

1336 **Supplemental Figure 1. N-cadherin mismatch control MO (MM)-treated embryos show**
1337 **normal trigeminal ganglion morphology.** (A-A') Representative images of the trigeminal
1338 ganglion after Tubb3 immunostaining (E4.5/HH23-25, (n=4)). Scale bar in (A) is 250 μm and applies
1339 to (A'). (B) Mean whole trigeminal ganglia area ± SEM for contralateral control and N-cadherin MM
1340 sides of embryos. Statistical significance was determined via an unpaired t-test. Abbreviations: TG:
1341 trigeminal ganglion; OpV: ophthalmic; MmV: maxillomandibular; MM: mismatch control; MO:
1342 morpholino; ns: not significant.

1343

1344 **Supplemental Figure 2: N-cadherin knockdown in placode cells does not increase cell**
1345 **proliferation at later developmental stages.** (A) Immunoblots of E6.5/HH28-30 electroporated
1346 (MO) and contralateral (CNTL) trigeminal OpV lobes for N-cadherin, phospho-histone H3 (PHH3),
1347 and GAPDH (n=2). (B) Protein levels of N-cadherin and phospho-histone H3 normalized against
1348 GAPDH loading control, presented as a fraction of total signal from contralateral control OpV
1349 lobes.

1350

1351 **Supplemental Figure 3: N-cadherin depletion from placode cells does not alter**
1352 **subpopulations of sensory neurons within the trigeminal ganglion.** (A-D') Sagittal serial
1353 sections through the OpV lobe of the trigeminal ganglion (contralateral control (A-B') and N-
1354 cadherin MO-electroporated side (C-D')) from representative E5.5/HH26-27 (n=4) embryos with
1355 TrkA and TrkB immunostaining. Images of TrkA and TrkB serial sections were merged to generate
1356 representative images. Scale bar in (A) is 100 μm and applies to (C); scale bar in (B) is 50 μm and
1357 applies to (B, D-D'). (E) Average number of TrkA- or TrkB-positive OpV neurons ± SEM after N-
1358 cadherin MO electroporation. (F) Average number of TrkA- or TrkB-positive OpV neurons
1359 normalized against OpV lobe area ± SEM. Statistical significance was determined via paired t-tests
1360 (E, F). (*) $p<0.05$.

1361

1362 **Supplemental Figure 4. Sequential electroporation of neural crest cells and placode cells**
1363 **exclusively labels distinct cell populations**. Representative images of an HH25/E4.5 embryo
1364 sequentially electroporated with PiggyBacGFP plus PBase (neural crest cells) and N-cadherin MM
1365 (placode cells), followed by Tubb3 and GFP immunostaining. Scale bar in (A) is 100 μm and scale
1366 bar in (B) is 50 μm and applies to (B'-B'').

1367

1368 **Supplemental Figure 5. N-cadherin MO-treated explants qualitatively exhibit less neural**
1369 **crest-derived axon outgrowth.** (A-B') Representative images of sequentially-electroporated
1370 trigeminal explants with neural crest cells co-electroporated with PiggyBacGFP plus PBase, and
1371 placode cells electroporated with N-cadherin MM (A-A') or N-cadherin MO (B-B'), followed by GFP

1372 and Tubb3 immunostaining. Arrowheads in (A') and (B') point to neural crest-derived axons. Scale
1373 bar in (A) is 100 μm and applies to all images.

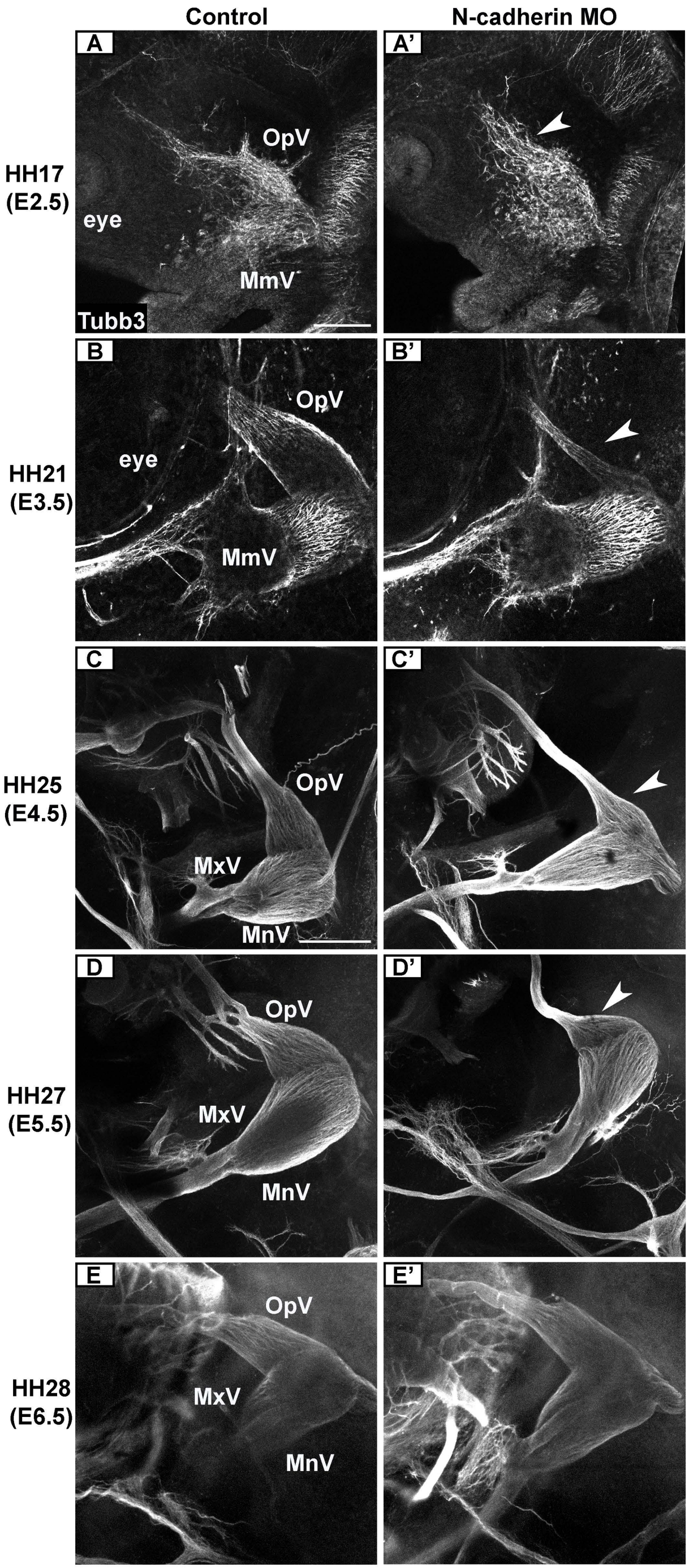
Control
N-cadherin MO
A
A'
HH17
(E2.5)
OpV
eye
MmV
Tubb3
B
B'
HH21
(E3.5)
OpV
eye
MmV
C
C'
HH25
(E4.5)
OpV
MxV
MnV
D
D'
HH27
(E5.5)
OpV
MxV
MnV
E
E'
HH28
(E6.5)
OpV
MxV
MnV

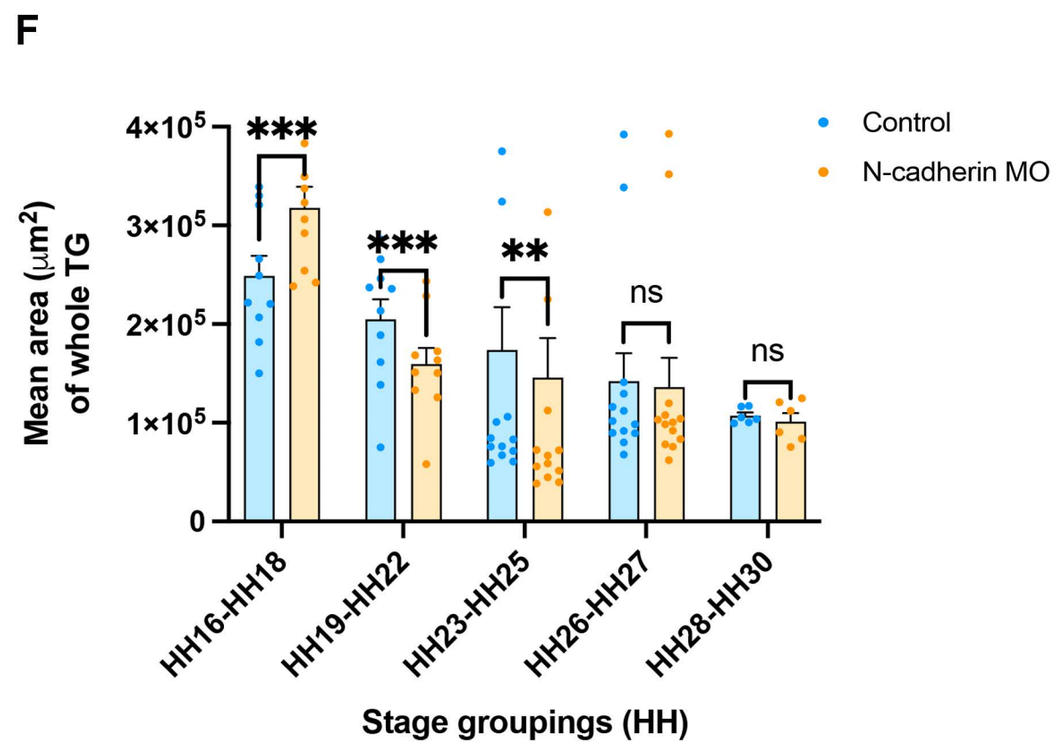
F
Control
N-cadherin MO
Mean area (μm²) of whole TG
4×10⁵
3×10⁵
2×10⁵
1×10⁵
0
***
***
**
ns
ns
HH16-HH18
HH19-HH22
HH23-HH25
HH26-HH27
HH28-HH30
Stage groupings (HH)

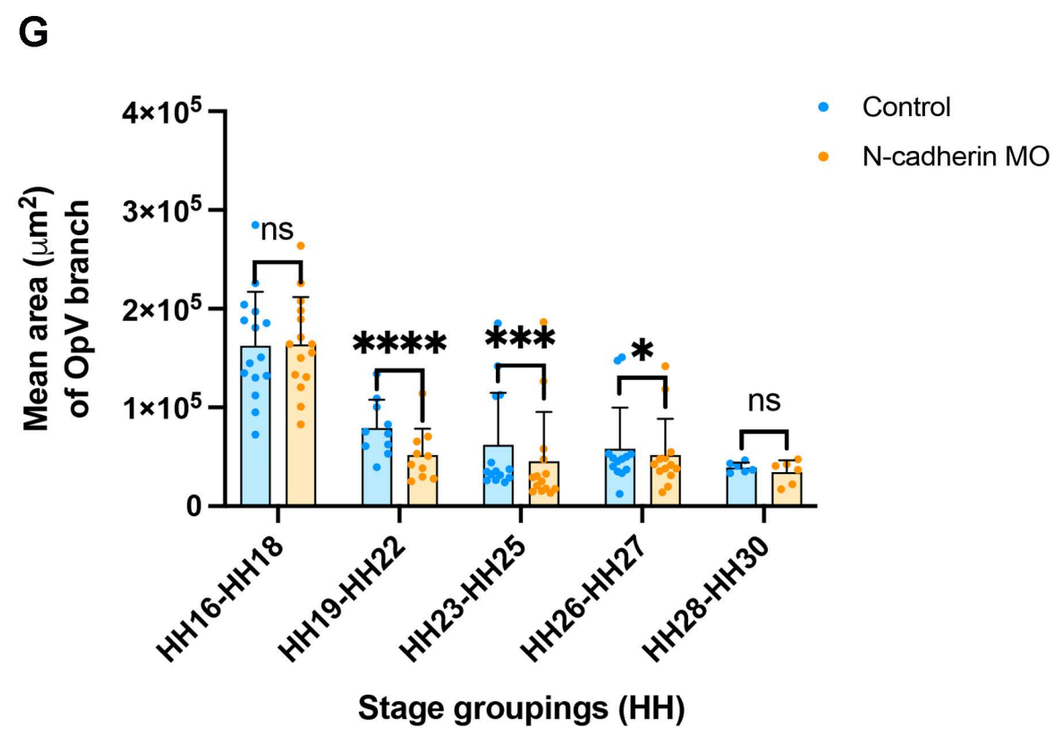
G
Control
N-cadherin MO
Mean area (μm²) of OpV branch
4×10⁵
3×10⁵
2×10⁵
1×10⁵
0
ns
****
***
*
ns
HH16-HH18
HH19-HH22
HH23-HH25
HH26-HH27
HH28-HH30
Stage groupings (HH)

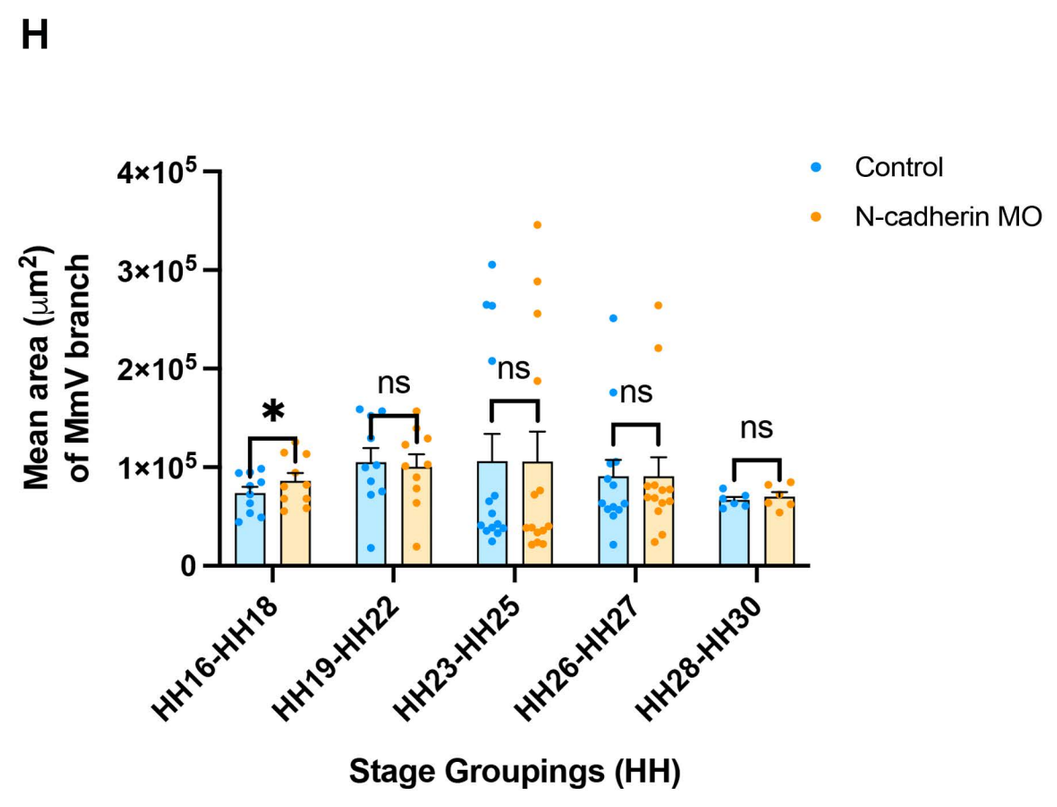
H
Control
N-cadherin MO
Mean area (μm²) of MmV branch
4×10⁵
3×10⁵
2×10⁵
1×10⁵
0
*
ns
ns
ns
ns
HH16-HH18
HH19-HH22
HH23-HH25
HH26-HH27
HH28-HH30
Stage Groupings (HH)

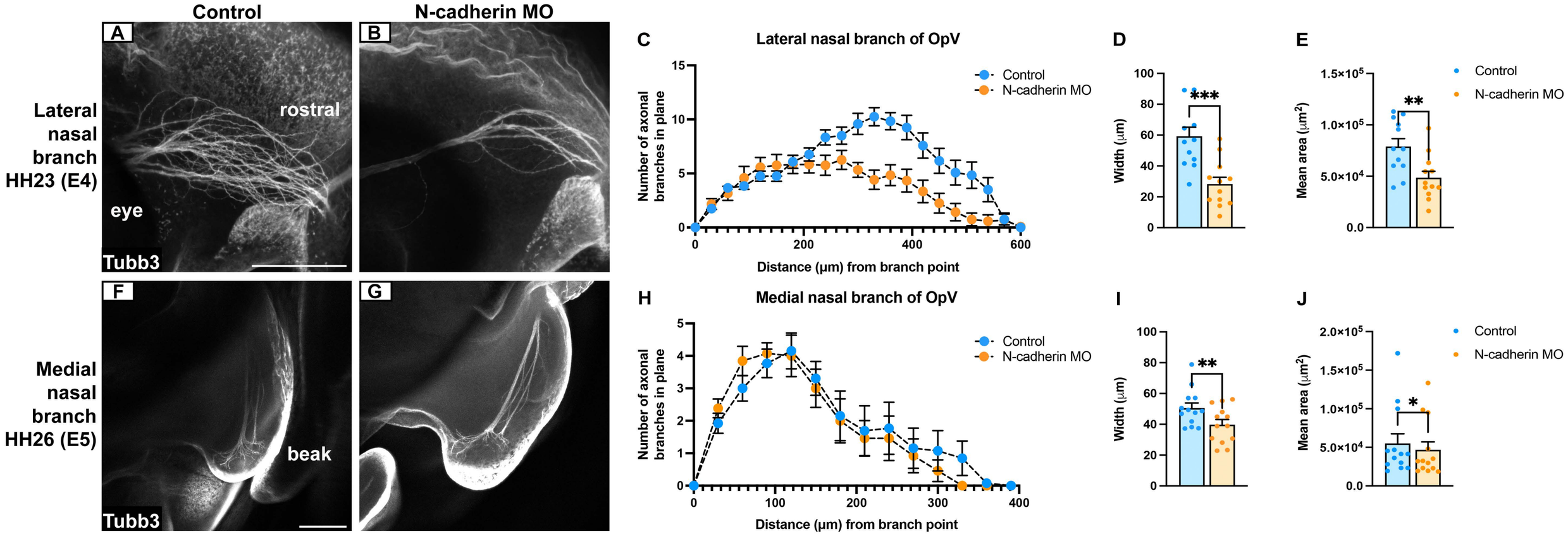
Control
N-cadherin MO
A
B
Lateral nasal branch HH23 (E4)
rostral
eye
Tubb3
F
G
Medial nasal branch HH26 (E5)
beak
Tubb3
C
Lateral nasal branch of OpV
Number of axonal branches in plane
Distance (μm) from branch point
Control
N-cadherin MO
D
Width (μm)
***
E
Mean area (μm²)
**
H
Medial nasal branch of OpV
I
**
J
*

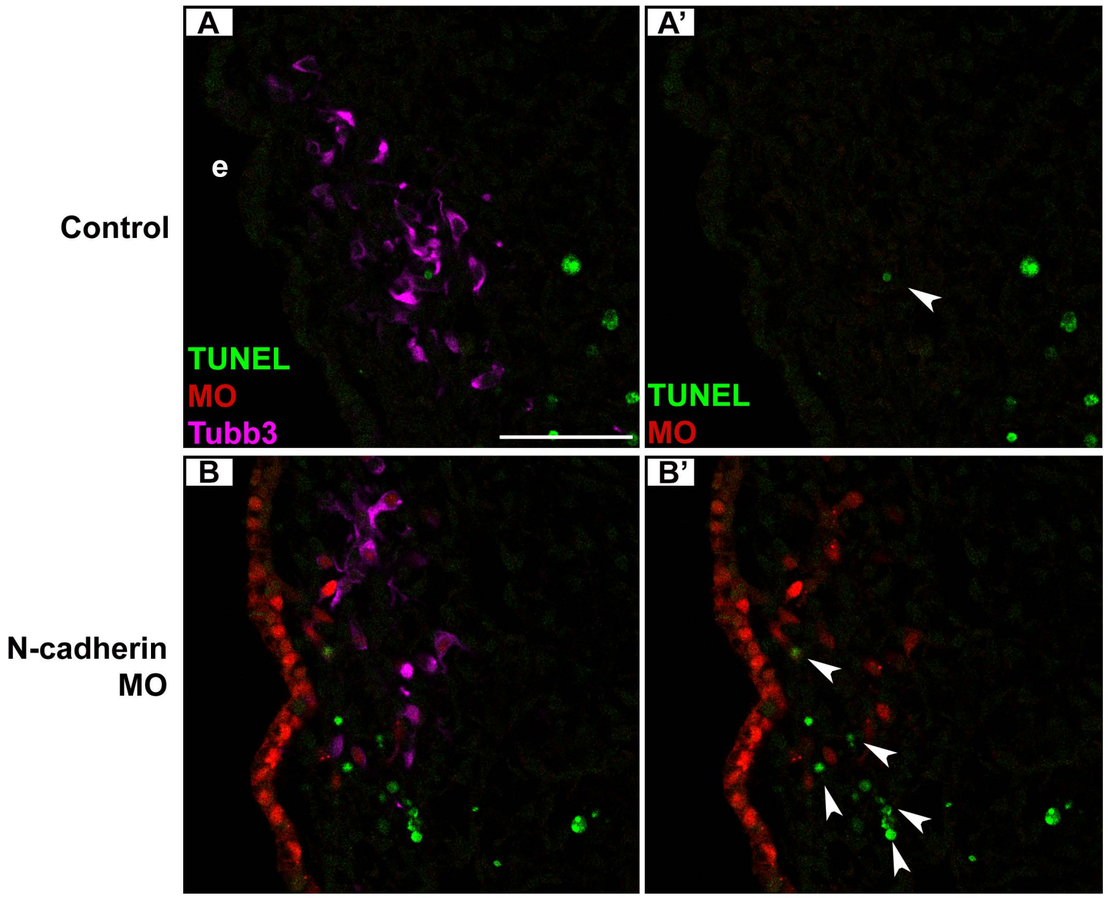
A
A'
e
Control
TUNEL
MO
Tubb3
TUNEL
MO
B
B'
N-cadherin
MO

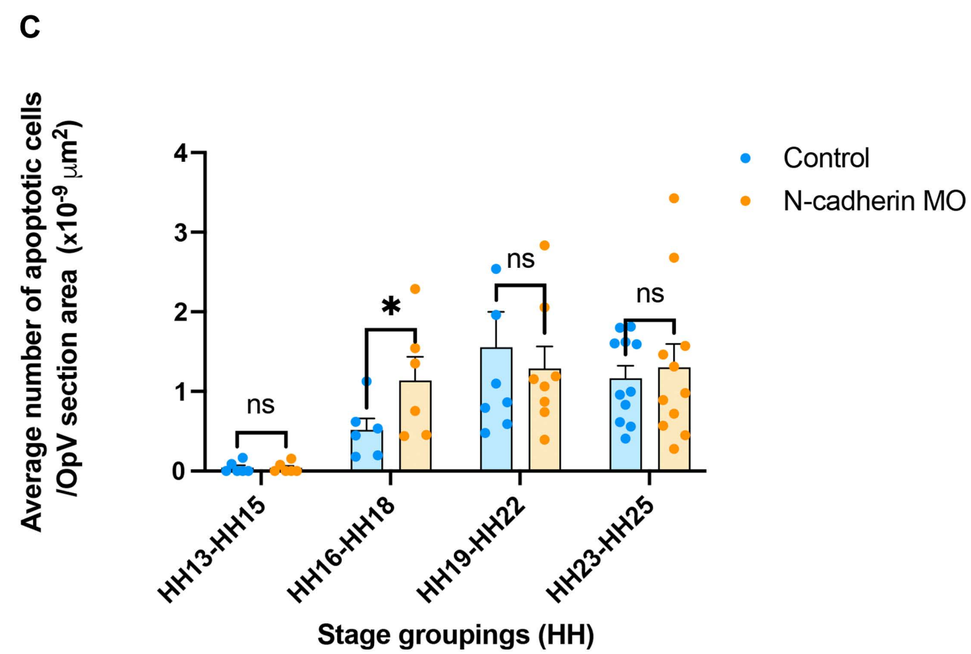
C
Average number of apoptotic cells
/OpV section area (x10-9 µm2)
4
3
2
1
0
ns
*
ns
ns
HH13-HH15
HH16-HH18
HH19-HH22
HH23-HH25
Stage groupings (HH)
Control
N-cadherin MO

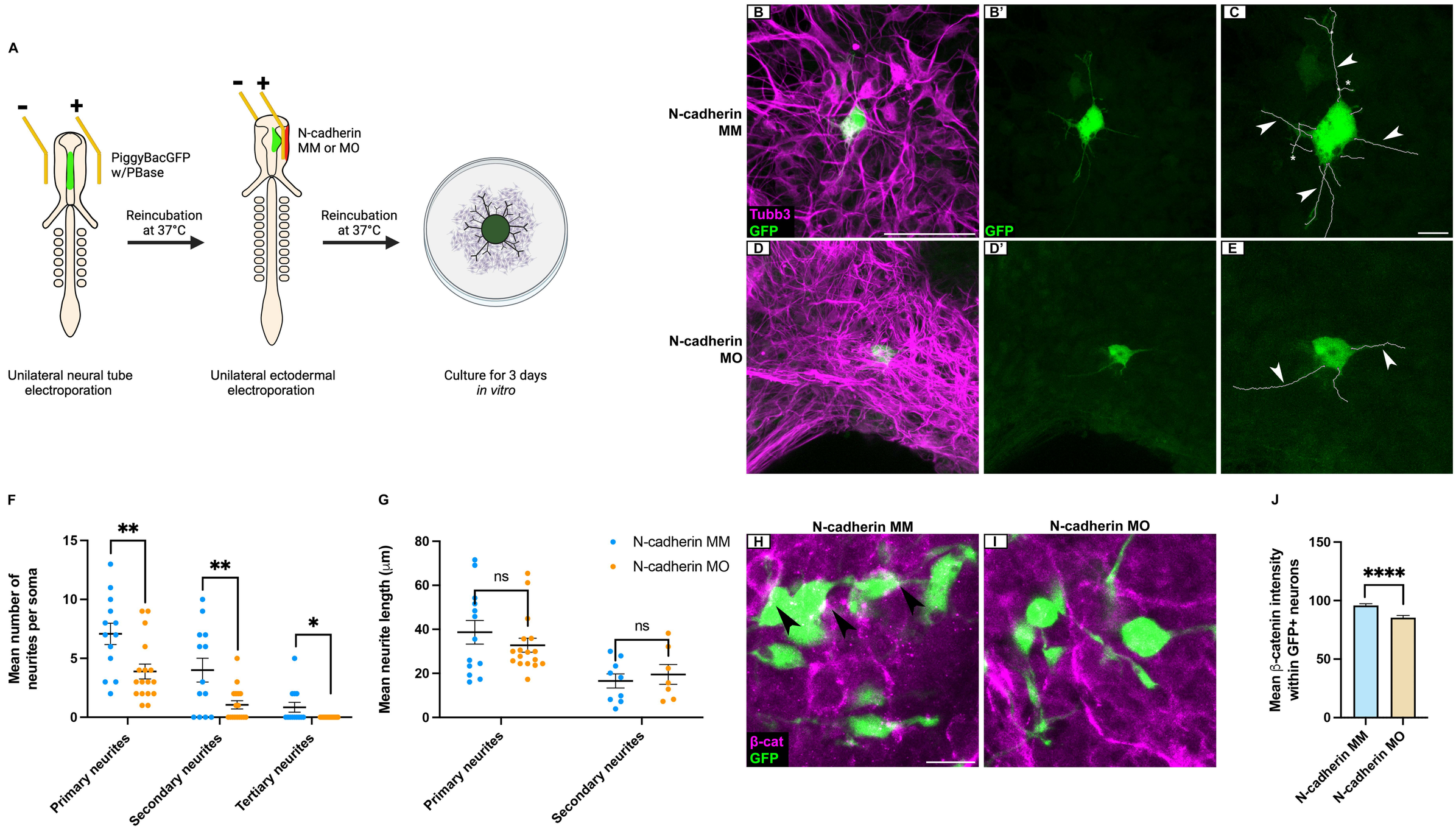
A
PiggyBacGFP w/PBase
Reincubation at 37°C
N-cadherin MM or MO
Reincubation at 37°C
Unilateral neural tube electroporation
Unilateral ectodermal electroporation
Culture for 3 days in vitro
N-cadherin MM
N-cadherin MO
B
B'
C
D
D'
E
Tubb3
GFP
GFP
F
Mean number of neurites per soma
Primary neurites
Secondary neurites
Tertiary neurites
G
Mean neurite length (μm)
ns
ns
N-cadherin MM
N-cadherin MO
H
I
β-cat
GFP
J
Mean β-catenin intensity within GFP+ neurons
****
N-cadherin MM
N-cadherin MO

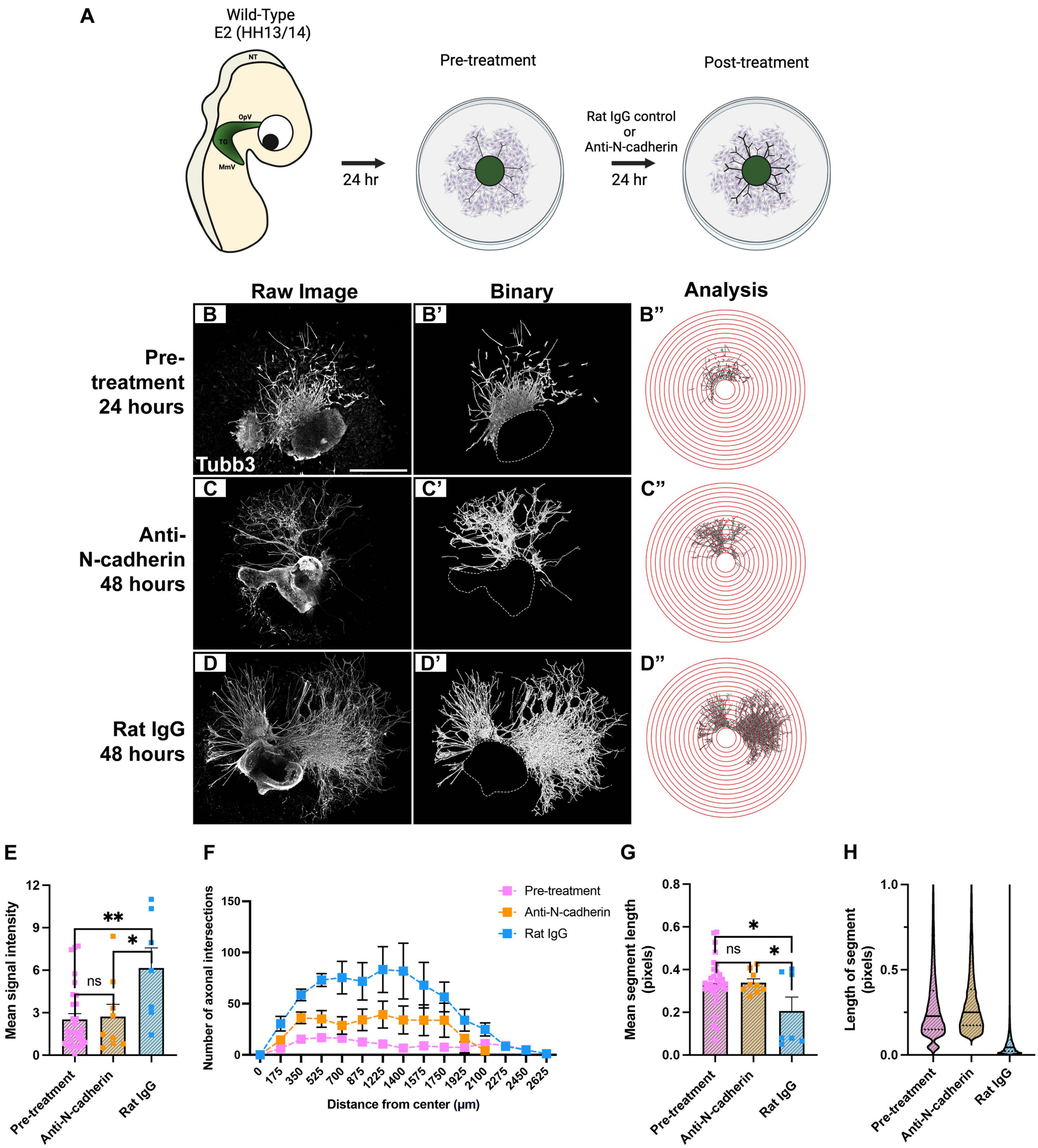
A
Wild-Type
E2 (HH13/14)
NT
OpV
TG
MmV
24 hr
Pre-treatment
Rat IgG control
or
Anti-N-cadherin
24 hr
Post-treatment
Raw Image
Binary
Analysis
Pre-treatment 24 hours
Anti-N-cadherin 48 hours
Rat IgG 48 hours
B
B'
B''
C
C'
C''
D
D'
D''
Tubb3
E
Mean signal intensity
**
*
ns
Pre-treatment
Anti-N-cadherin
Rat IgG
F
Number of axonal intersections
Pre-treatment
Anti-N-cadherin
Rat IgG
Distance from center (µm)
G
Mean segment length (pixels)
*
ns
*
H
Length of segment (pixels)

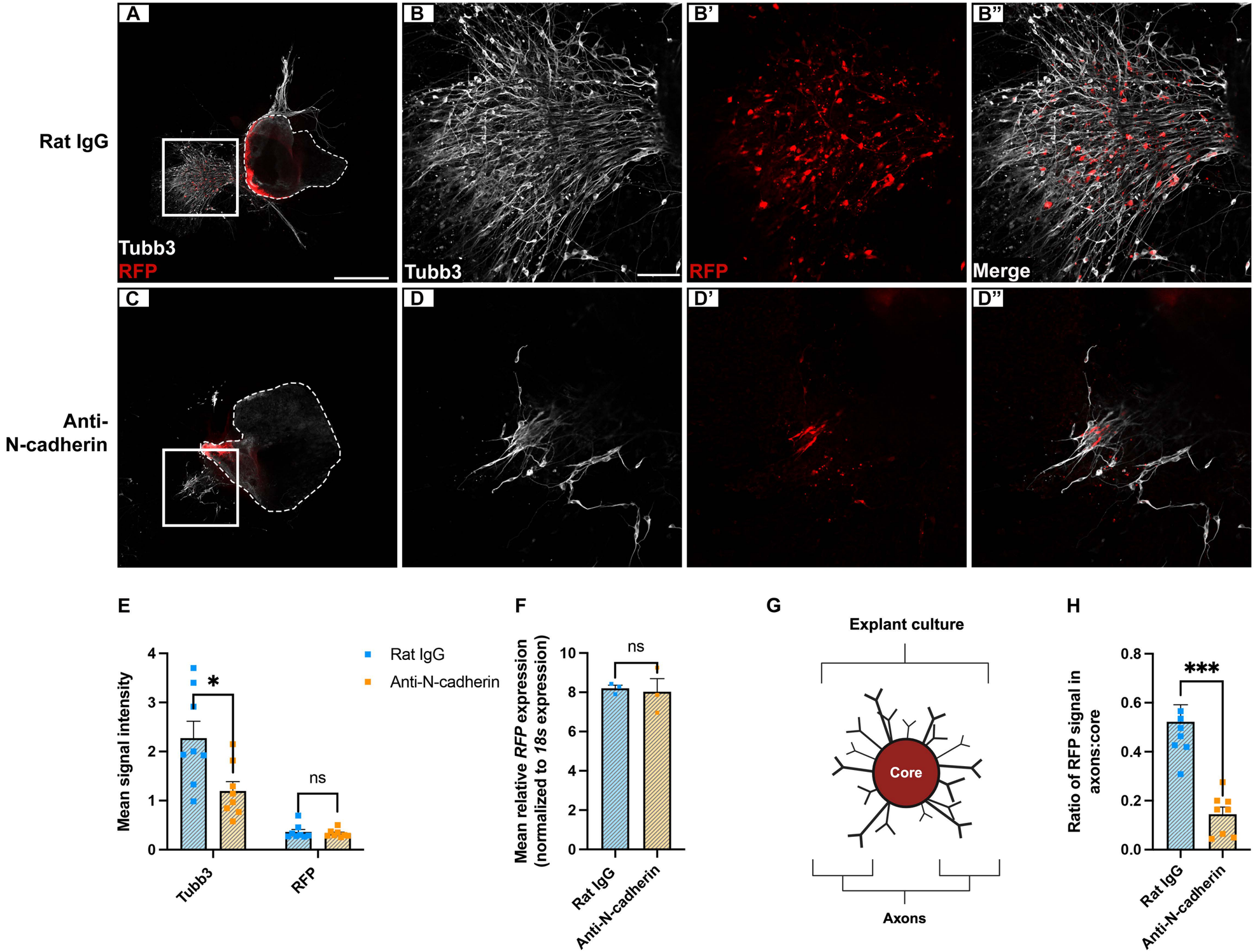
Rat IgG
Anti-
N-cadherin
A
Tubb3
RFP
B
Tubb3
B'
RFP
B''
Merge
C
D
D'
D''
E
Mean signal intensity
Rat IgG
Anti-N-cadherin
*
ns
Tubb3
RFP
F
Mean relative RFP expression
(normalized to 18s expression)
ns
Rat IgG
Anti-N-cadherin
G
Explant culture
Core
Axons
H
Ratio of RFP signal in
axons:core
***
Rat IgG
Anti-N-cadherin

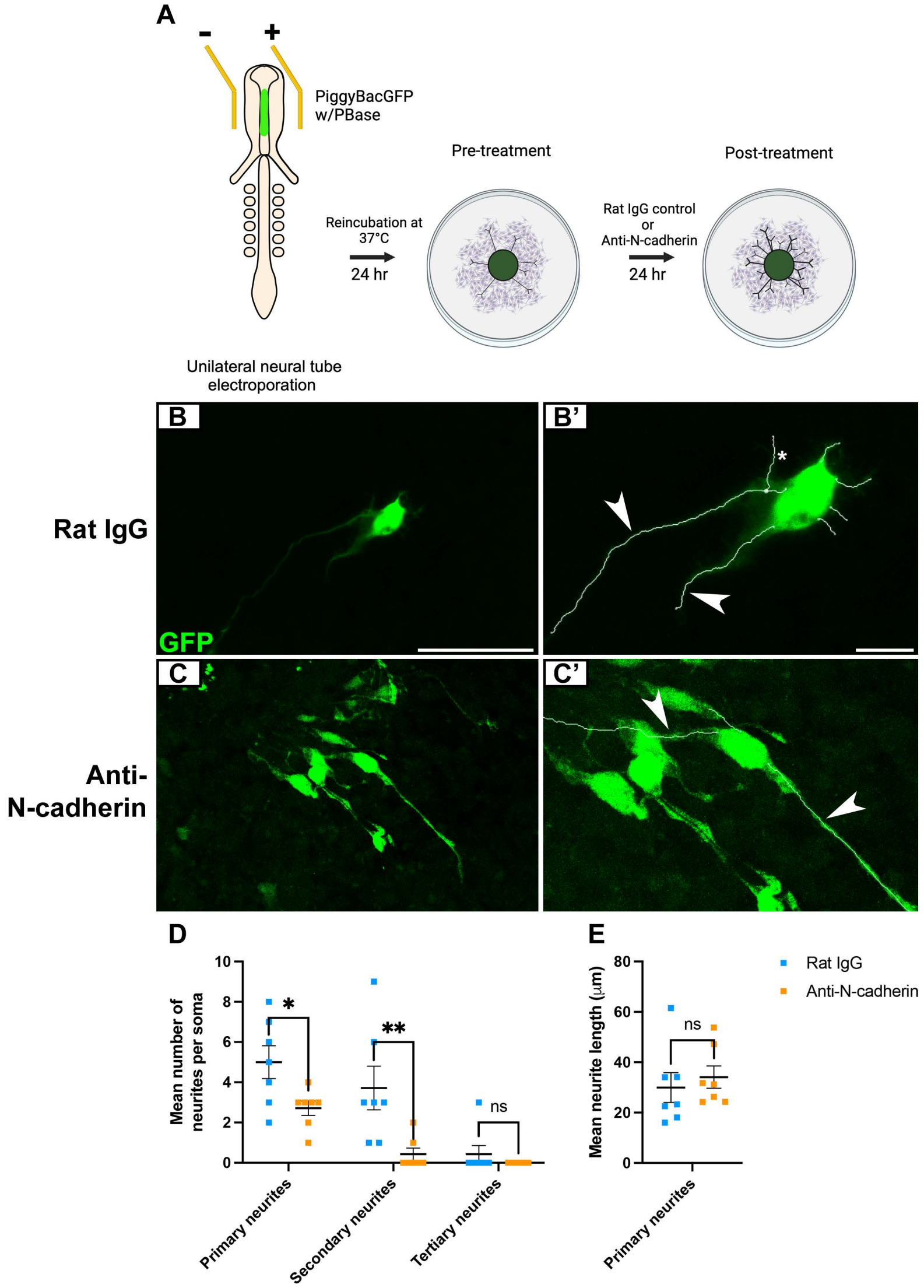
A
-
+
PiggyBacGFP
w/PBase
Unilateral neural tube
electroporation
Reincubation at
37°C
24 hr
Pre-treatment
Rat IgG control
or
Anti-N-cadherin
24 hr
Post-treatment
Rat IgG
Anti-
N-cadherin
B
B'
C
C'
GFP
D
Mean number of
neurites per soma
10
8
6
4
2
0
*
**
ns
Primary neurites
Secondary neurites
Tertiary neurites
E
Mean neurite length (μm)
80
60
40
20
0
ns
Primary neurites
Rat IgG
Anti-N-cadherin